Faculty of Electrical and Electronic Engineering Technology

INITIAL DEVELOPMENT OF A NANOELECTRONIC BIOSENSOR FOR UREA DETECTION

MUHAMMAD AKMAL BIN ABD WAHID

Bachelor of Electronics Engineering Technology (Telecommunications) with Honours

2023

INITIAL DEVELOPMENT OF A NANOELECTRONIC BIOSENSOR FOR UREA DETECTION

MUHAMMAD AKMAL BIN ABD WAHID

A project report submitted
in partial fulfillment of the requirements for the degree of
Bachelor of Electronics Engineering Technology (Telecommunications) with Honours

Faculty of Electrical and Electronic Engineering Technology

UNIVERSITI TEKNIKAL MALAYSIA MELAKA

2023

DECLARATION

I declare that this project report entitled “Initial Development of A Nanoelectronic Biosensor for Urea Detection” is the result of my own research except as cited in the references. The project report has not been accepted for any degree and is not concurrently submitted in candidature of any other degree.

Signature : 

Student Name : MUHAMMAD AKMAL BIN ABD WAHID

Date : 20/2/2023

APPROVAL

I hereby declare that I have checked this project report and in my opinion , this project report is adequare in terms of scope and quality for the awared of the degree of Bachelor of Electronics Engineering Technology (Telecommunications) with Honors.

Signature : 

NAJMIAH RADIAH BINTI MOHAMAD
Pensyarah Kanan
Jabatan Teknologi Kejuruteraan Elektronik dan Komputer
Fakulti Teknologi Kejuruteraan Elektrik dan Elektronik
Universiti Teknikal Malaysia Melaka

Supervisor Name : NAJMIAH RADIAH BINTI MOHAMAD

Date : 24/2/23

DEDICATION

To my beloved mother, Siti Fatimah Binti Shabuddin, and father,Abdul Wahid Haji Othman, thank you for supporting me when I continue my studies for bachelor degree in UTeM.

To my siblings, Sahil Aziz Bin Abd Wahid and Nur Annira Binti Abd Wahid and my classmates , thank you for providing creativity expertise and suggestion for completing this project.

To my friends Mohammad Iffad Hakim Bin Mohammad Zahair , Mohammad Irsyad Hakim Bin Mohammad Zahair ,Muhd Nabil bin Hashim ,Muhd Hakimi bin Ismail ,Muhammad Isamuddin bin Zani and Muhammad Suhaimi bin Samion , thank you for supporting me when I'm continuing my studies for bachelor degree in UTeM.

To my supervisor, Madam Najmiah Radiah binti Mohamad, thank you for your dedication, organization, enthusiasm and hardwork .You're an inspiring lecturer. Thanks for making me brave.

Thank you everyone for the emotional support.

ABSTRACT

A nanoelectronic biosensor for urea detection often employs a nanomaterial as the sensing element, such as carbon nanotubes or graphene. The nanomaterial is functionalized with a biomolecule, such as an enzyme that binds urea more selectively. The binding of urea to the biomolecule changes the electrical characteristics of the nanomaterial, which are evaluated by electrochemical impedance spectroscopy or cyclic voltammetry. However, biosensor development has a detection limit, a detection time, and specificity. Detection time introduces significant challenges when designing biosensor systems, such as finding a suitable technology while maintaining the highest sensitivity and specificity. They can also be affected by environmental changes and contamination. In this research, a Polypyrrole (PPY)/Multiwalled Carbon Nanotube (MWCNT) nanofilm is fabricated by using choronoamperometry. This fabricated PPy/MWCNT nanofilm is characterised by using Fourier transform infrared spectroscopy (FTiR), scanning electron microscopy (SEM), and X-ray diffraction (XRD) to check the morphology and analyse the material's properties. Then, the relationship between voltage and current is analysed using the cyclic voltammetry method. The electrodeposition and cyclic voltammetry methods have been used with the AutoLAB potentiostat and NOVA 2.0 AutoLAB software. Based on the chronoamperometry results on PPY/MWCNT for 1-minute results, the carbon electrode has the highest current at 0.001A. The result changes after a longer chronoamperometry process. For chronoamperometry on PPY/MWCNT for 3-minute results, the copper electrode has the highest current at 0.0011 A, followed by the stainless steel electrode at 0.001 A. Lastly, for chronoamperometry on PPY/MWCNT for 5-minute results, the copper electrode maintained the highest current at 0.0011 A, followed by the aluminium electrode at 0.0009A. The cyclic voltammetry of carbon and stainless steel has been set between -0.8 V and +0.4 V. After the repititive potential cycles, the major difference between this two solution which are PBS solution and urea solution are the current. Based on the cyclic voltammetry results, the current in the PBS solution for carbon is -0.0025 A and the current in the analyte (representing urea) solution for carbon is -0.0037 A. Then, the current in the PBS solution for stainless steel is -0.0010 A, and the current in the analyte solution for stainless steel is -0.0015 A. As a conclusion, the changes in current for both PBS and analyte solutions show that the biosensor has been successfully developed .

ABSTRAK

Biosensor nanoelektronik untuk pengesanan urea selalunya menggunakan bahan nano sebagai elemen penderiaan, seperti tiub nano karbon atau graphene. Bahan nano difungsikan dengan biomolekul, seperti enzim yang mengikat urea dengan lebih selektif. Pengikatan urea kepada biomolekul mengubah ciri elektrik bahan nano, yang dinilai oleh spektroskopi impedans elektrokimia atau voltammetri kitaran. Walau bagaimanapun, pembangunan biosensor mempunyai had pengesanan, masa pengesanan dan kekhususan. Masa pengesanan memperkenalkan cabaran penting apabila mereka bentuk sistem biosensor, seperti mencari teknologi yang sesuai sambil mengekalkan kepekaan dan kekhususan tertinggi. Mereka juga boleh terjejas oleh perubahan persekitaran dan pencemaran. Dalam penyelidikan ini, sebuah nanofilem Polypyrrole (PPY)/Multiwalled Carbon Nanotube (MWCNT) dibuat dengan menggunakan koronoamperometri. Nanofilem PPy/MWCNT rekaan ini dicirikan dengan menggunakan spektroskopi inframerah transformasi Fourier (FTiR), mikroskop elektron pengimbasan (SEM), dan pembelauan sinar-X (XRD) untuk memeriksa morfologi dan menganalisis sifat bahan. Kemudian, hubungan antara voltan dan arus dianalisis menggunakan kaedah voltammetri kitaran. Kaedah elektrodeposisi dan voltammetri kitaran telah digunakan dengan perisian AutoLAB potentiostat dan NOVA 2.0 AutoLAB. Berdasarkan keputusan kronoamperometri pada PPY/MWCNT untuk keputusan 1 minit, elektrod karbon mempunyai arus tertinggi pada 0.001A. Hasilnya berubah selepas proses kronoamperometri yang lebih panjang. Untuk chronoamperometry pada PPY/MWCNT untuk keputusan 3 minit, elektrod kuprum mempunyai arus tertinggi pada 0.0011 A, diikuti oleh elektrod keluli tahan karat pada 0.001 A. Akhir sekali, untuk chronoamperometry pada PPY/MWCNT untuk keputusan 5 minit, elektrod kuprum mengekalkan arus tertinggi pada 0.0011 A, diikuti oleh elektrod aluminium pada 0.0009A. Voltammetri kitaran karbon dan keluli tahan karat telah ditetapkan antara -0.8 V dan +0.4 V. Selepas kitaran potensi repititif, perbezaan utama antara kedua-dua larutan ini iaitu larutan PBS dan larutan analit (mewakili urea) adalah arus. Berdasarkan keputusan voltammetri kitaran, arus dalam larutan PBS untuk karbon ialah -0.0025 A dan arus dalam larutan larutan analit (mewakili urea) untuk karbon ialah -0.0037 A. Kemudian, arus dalam larutan PBS untuk keluli tahan karat ialah -0.0010 A, dan arus dalam larutan analit untuk keluli tahan karat ialah -0.0015 A. Sebagai kesimpulan, perubahan arus untuk kedua-dua larutan PBS dan glukosa menunjukkan bahawa biosensor telah berjaya dibangunkan.

ACKNOWLEDGEMENT

To complete this project, many people had helped and inspired me. I have received a lot of support from each of them.

First and foremost, I would like to express my gratitude to my supervisor, PUAN NAJMIAH RADIAH BINTI MOHAMAD for their precious guidance, words of wisdom and patient throughout this project.

I am also my fellow colleague and housemates for the willingness of assisting me regarding the project. They are never relentless to share their knowledge, information, and experience with me.

My highest appreciation goes to my parents, and family members for their love and prayer during the period of my study.

An honorable mention also goes to both of my long-time friends for brainstorming together to form this project idea.

TABLE OF CONTENT

LIST OF TABLES

LIST OF FIGURES

LIST OF SYMBOLS

μ	-	Micro

LIST OF ABBREVIATIONS

V	-	Voltage
SPR	-	Surface Plasmon Resonanse
FET	-	Field-Effect Biosensor
AuNPs	-	Gold nanoparticles
DNA	-	Deoxyribonucleic Acid
QCM	-	Quartz Crystal Microbalance
MHz	-	Megahertz
ng/ml	-	Nanograms per Milliliter
fg/ml	-	Femtogram per Molliliter
pH	-	Potential of Hydrogen
MoS_2	-	Molybdenum Disulphide
EGFET	-	Extended Gate Field Effect Transistor
PPy	-	Polypyrrole
MBs	-	Magnetic Beads
GO	-	Graphene Oxide
NiO	-	Nickel Oxide
LED	-	Light-Emitting Diode
MTM	-	Multi-mode Thincore Multi-mode
Ag NPs	-	Silver nanoparticle
RuO2	-	Ruthenium(IV) oxide
T	-	Time
mV	-	Millivolt
FWHM	-	Full Width at Half Maximum
FDTD	-	Finite-difference time-domain
CO2	-	Carbon dioxide
SEM	-	Scanning Electron Microscope
XRD	-	X-ray diffraction
FTIR	-	Fourier-transform infrared spectroscopy
Cm	-	Centimeter
DAFc	-	Direct alcohol fuel cells
SnS	-	Stannous sulphide
MLG	-	Multilayered graphene
REFET	-	Reference field effect transistors
EnFET	-	Enzyme field effect transistors

INTRODUCTION

1.1 Background

Biosensor research and development is becoming a hot issue since they are simple, rapid, and low-cost. They enable improvements in point-of-care applications like disease marker detection. Surface chemistry advances have opened up a slew of new possibilities for constructing target molecule identification systems. New transducers, as well as the downsizing and integration of high-throughput biosensors, are expected to be developed as a result of nanofabrication advances.

1.2 Problem Statement

For urea determination, a number of approaches have been developed, including direct and indirect detection. The chromatographic and colorimetric techniques for urea testing are reliable and have been widely utilised for general monitoring. These procedures, on the other hand, need time-consuming sample preparation and/or expensive equipment, rendering them unsuitable for online or onsite monitoring [1]. For many therapeutically important targets and qualitative or semi-quantitative outcomes, certain traditional biosensors have relatively low sensitivity [2] . However, the clinical application of biosensing devices has not yet reached this level, and there are several significant scientific and technological obstacles that must be overcome before the devices can be manufactured and used on a large scale [3].

1.3 Project Objective

This project's major objective is to develop a nanoelectronic biosensor for urea detection. The following below are the specific objectives:

a) To fabricate PPy/MWCNT nanofilm using chronoamperometry .
b) To characterize PPy/MWCNT at nanofilm using Fourier Transform Infrared Spectroscopy (FTIR), Scanning Electron Microscope (SEM), and X-Ray Diffreaction (XRD).

c) To analyze the relationship between voltage and current for different materials of electrodes during analyte detection.

1.4 Scope of Project

To avoid any ambiguity about the project's scope owing to various limits and constraints, the project's scope is stated as follows:

a) Study the relationship between the voltage, current and the surface area by using cyclic voltammetry method
b) Design and simulate the experiment using software for simulation electrochemistry.
c) Comparing the electrodes on which is better at sensitivity for detecting urea based on sensorgram results.
d) Electrodeposition and cyclic voltammetry are experimented by using AutoLAB potentiostat with NOVA 2.0Autolab software.
e) Using different types of electrodes materials such as copper , carbon , aluminum and stainless steel.
f) Using PBS and urea solution for cyclic voltammetry process.

CHAPTER 2

LITERATURE REVIEW

1.5 Introduction to Biosensor

A biosensor is analytical tool made up from two main parts: an immobilised biocomponent and a transducer that converts to a detectable electrical signal from a biological signal . The fact that urea is toxic in excess of certain levels underscores the importance of this research, and continuous real-time monitoring in environmental, clinical, and food-related settings is critical. Traditional analytical processes are time consuming and often laboratory restricted, but biosensors provide the advantages of ease of use, mobility, and the potential to deliver real-time information. Biosensor research and development became the most widely studied discipline because easy,rapid, and low-cost biosensors contribute to advances in next-generation medicines such as individualised medicine and ultrasensitive point-of-care detection of disease markers.

This chapter evaluated traditional biosensors and biosensing techniques from the perspective of smart biomaterials, focusing on recent developments in important biosensors such as SPR-based biosensors, FET-based biosensors, and AuNPs-based biosensors. The various techniques for immobilising the urease enzyme, the stability and response time characteristics, and the transducers used in biosensor development are all summarised in this review. The case examples presented here clearly show that biosensor research is really interdisciplinary. Improvements in nanofabrication technology also promise the development of novel transducers as well as the downsizing and integration of high-throughput biosensors. Multidisciplinary efforts outside of typical specialisations are required for the development of novel biosensors. As a result of the fusion of significant interdisciplinary talent, biosensor development will be expedited and biological domains will be revolutionised [4].

1.6 Purpose of biosensor

A biosensor is a device that assesses biological or chemical reactions by using signals proportional to the concentration of an analyte in a reaction. Biosensors are utilised in illness

monitoring, drug discovery,disease monitoring, and disease indicators in physiological fluids such as blood, urine, saliva, sweat [4].

Bioreceptor: Bioreceptor is a molecule that uniquely recognises the analyte. Enzymes, cells, deoxyribonucleic acid (DNA), and antibodies are one of the examples of bioreceptor. When a bioreceptor interacts with an analyte, a signal is generated in form of light, pH or mass change [4].

Transducer: A device that converts one form of energy into another is known as a transducer. The biosensor's transducer is in charge on translating the bio-recognition event into measurable signal also known process as signalisation [4].

Electronics: This is the part of a biosensor that processes and displays the signal that has been transduced. It consists of intricate electrical circuitry that performs signal conditioning activities like as amplification and digital signal conversion. The processed signals are then quantified by the biosensor's display device [4].

Display: A user interpretation system that generates intelligible numbers or curves. This component generally consists a mix of software and hardware that produces results that are easy to understand. The display output signal depends on the demands of end user like numeric, visual, tabular, or an image [4].

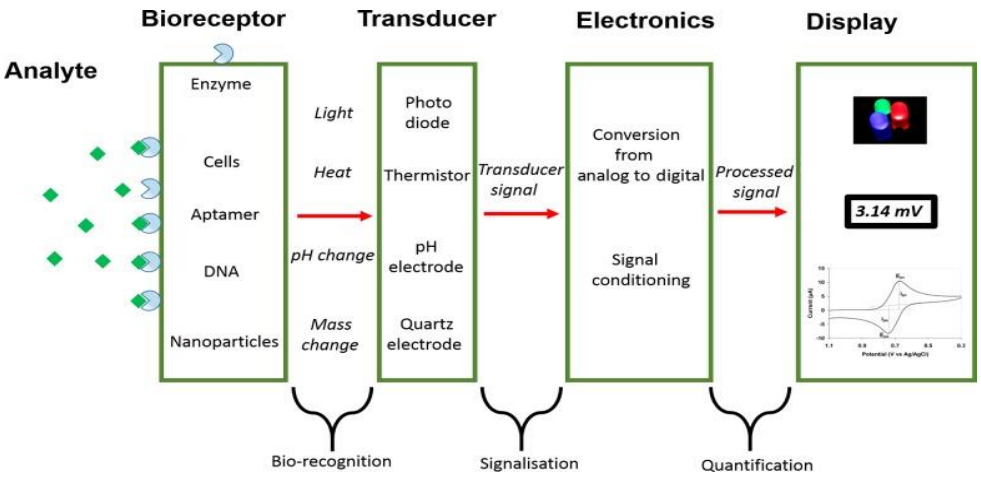

Figure 2.1 Schematic representation of biosensor[4]**.**

2.3 Principle of a biosensor

In most cases, the necessary biological material is in the form of an enzyme. By using an electroenzymatic method, which is a chemical process that uses a transducer to transform enzymes into matching electrical signals (typically current). One of the most often used The oxidation of the enzyme is the biological response [5].

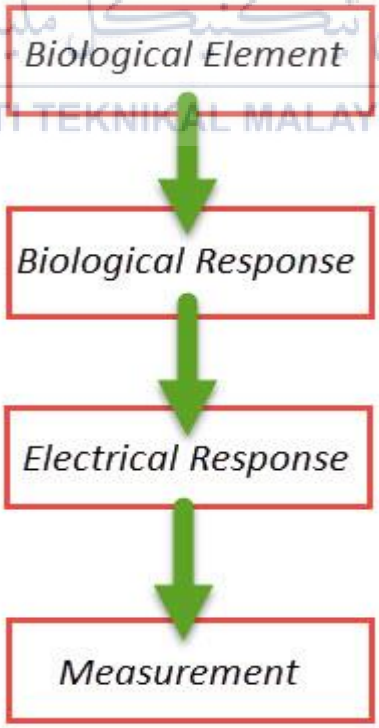

Figure 2.2 Principle of a Biosensor [5]**.**

Oxidation, which acts as a catalyst, changes the pH of the biological substance. Changes in pH have a direct impact on the enzyme's current carrying capacity, which is, once again, tied to the enzyme under investigation [5].

2.4 Types of Biosensor

There are two types of biosensors which use a biological element in the analysis and those who use a transduction mechanism. Some of the most often used biological elements or bio-recognition elements are DNA, enzymes, antibodies, bacteria, tissues, cell receptors, and other biological elements or bio-recognition elements.The kind of transduction employed in the sensor, i.e. the type of physiochemical coming from the sensing event, is the next and most often used categorization of Biosensors. Biosensors are further split into three categories based on the technique of transduction which is optical biosensor,mass-based biosensor and biosensor based from transduction element[5].

2.5 Optical Biosensor

Optical Fibers are crucial in the development of optical biosensors. The optical fibers enable for the identification of sensing elements using distinct light characteristics such as absorption, scattering, and fluorescence. Because the refractive index of the contacting surface varies, the reaction produces changes in any of the qualities described above. If the biological elements which are antibodies bonded to a metal layer, for example, refractive index of the medium that comes into contact with this layer will change. The fact that optical biosensors are non-electrical is one of their key benefits. By altering the wavelength of the light, they can evaluate many components on a single layer [5].

2.5.1 Surface Plasmon Resonance Based Biosensors

Due to the unique properties for real-time and label-free detection of biomolecular interactions, SPR based biosensors have emerged as crucial and valuable technologies during the last two decades. Due to its appealing sensing characteristics, light weight, compactness, and ease of implementation, SPR technology has many key applications in the

world of sensing. Enzyme detection, and protein–DNA hybridization are examples of SPR applications in biosensing, chemical, and environmental sensing [5].

2.6 Mass Based biosensors

Piezoelectric biosensor is analytical equipment that works on the basis of recording affinity interactions. A piezoelectric crystal is a sensor component that works on the basis of oscillations changing according to mass bound on the piezoelectric crystal surface. When mechanical force is applied, piezoelectric biosensors, create an electrical signal. The quartz crystal microbalance (QCM) model is an example of a piezoelectric biosensor. Figure 2.3 depicts the operating principle of QCM. The quartz crystal microbalance (QCM) is a widely used instrument in the electronics sector. These instruments are now utilized as attenuators in electrical equipment, with a fundamental mode frequency of 1–20 MHz Quartz crystal, which is equipped with metal electrodes, is the fundamental material utilized in the construction of the QCM sensor. The target analyte is detected in the environment using a sensitive coating material on the sensor surface. To convert the measured amount to an electrical signal, an adequate electronic circuit is required [5].

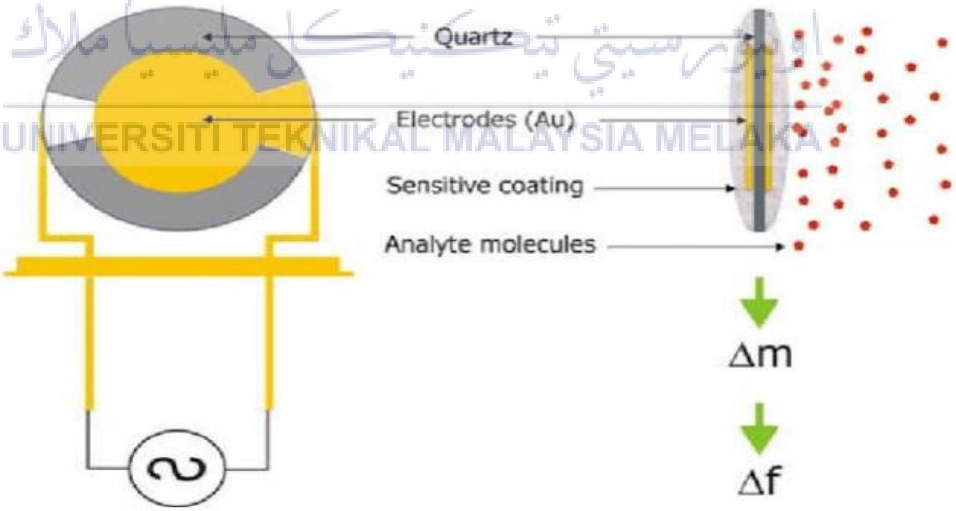

Figure 2.3 Working principle of Quartz Crystal Microbalance (QCM) sensor [5]**.**

2.7 Biosensors based on transduction element.

The type of transduction element utilized in the sensor is the most often used categorization for biosensors. Electrochemical biosensors, mass-based biosensors, and optical-based biosensors are the three primary kinds of biosensors. Each of these biosensors has a different operating principle and may thus be used in a range of applications. The many types of biosensors and their functioning processes are described briefly below. Some of the subclasses of biosensor types will also be described [5].

2.7.1 Electrochemical biosensors

Electrochemical biosensors evaluate the electrical potential difference generated by a contact between an analyte and membrane/sensor surface, and the best at detecting hybridized DNA, DNA binding medicines, urea content, and so on. The electrical potential difference and the logarithm of the material's electrochemically active concentration are proportional. Electrochemical biosensors have grown in popularity as an alternative to optical biosensors since they do not suffer from the numerous drawbacks that optical biosensors do. They provide a more consistent output, have a higher sensitivity, a faster reaction, and are less susceptible to interference. For sensing applications, electrochemical measurements are commonly used. Electrochemical biosensors are further categorized into several categories based on the electrical characteristics that they measure [5].

2.7.1.1 Conductometric biosensors

During a biological process, conductometric biosensors detect the electrical conductivity of the fluid. The total conductivity or resistivity of a solution varies when electrochemical processes create ions or electrons. They are less typically utilized in biosensing applications due to their low signal-to-noise ratio, especially when the biological receptor utilized is an enzyme. These biosensors, on the other hand, are nevertheless valuable for detecting affine interactions [5].

2.7.1.2 Potentiometric biosensors

Antigen/antibody interactions cause changes in pH and ion concentrations, which are measured using potentiometric biosensors. Despite the fact that potentiometric biosensors are the least prevalent of all biosensors, several methodologies for their creation have been discovered. The operating concept is based on the fact that when a voltage is applied to an electrode in solution, electrochemical processes produce current flow. The voltage at which these reactions take place denotes a specific reaction and analyte. Hu et al. used a microfluidic device with a light-addressable potentiometric sensor to track the metabolism of human breast cancer cells in real time [5].

2.7.1.3 Amperometric biosensors

This is perhaps the most widely utilized electrochemical detection approach in biosensors. This biosensor with a high sensitivity can identify electroactive species in biological test samples. When antigen/antibody pairing occurs, amperometric-based biosensors measure the change in current potentials during redox reactions. The Clark oxygen electrode is used in the majority of amperometric biosensors. Nakamura and colleagues developed amperometric biosensors for the indirect detection of E. coli. Brookes and colleagues developed another amperometric biosensor for the identification of Salmonella species [5].

2.7.1.4 Impedimetric biosensors

Impedimetric biosensors track changes in impedances when antigens and antibodies interact. Impedance, which often uses a circuit bridge as a measuring instrument, is highly suited for bacteria identification in clinical specimens, quality monitoring, and detecting particular food pathogens. Furthermore, these biosensors can be used to regulate industrial microbial operations [5].

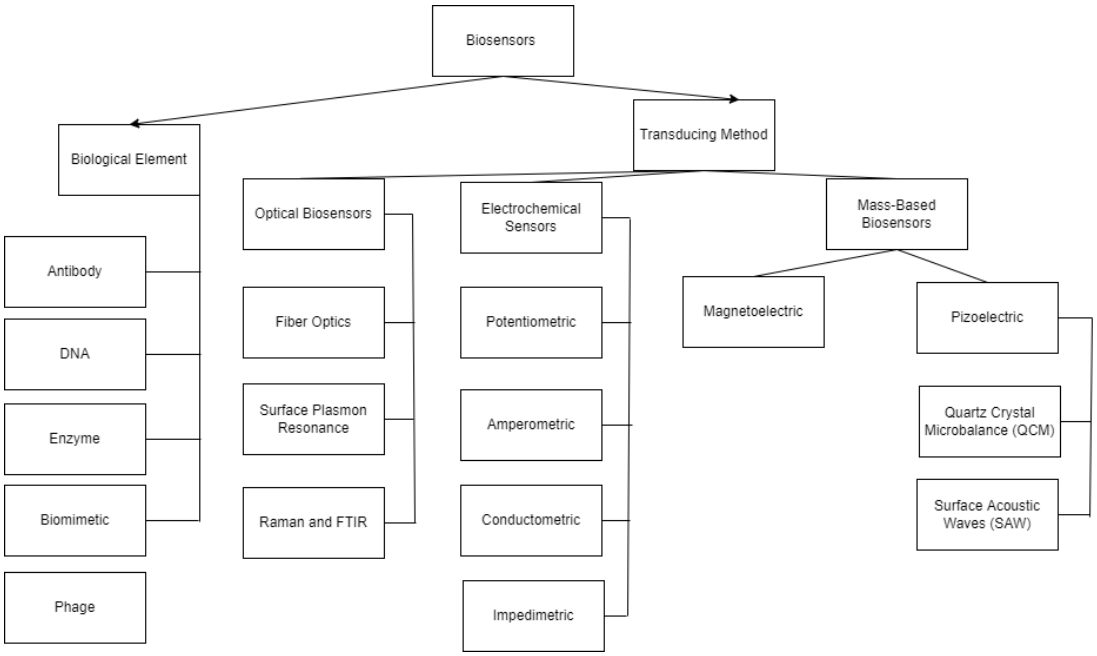

Figure 2.4 Types of Biosensor [5]**.**

2.8 Important characteristics of a biosensors

Certain aspects need to be considered while creating a biosensor. The performance and utility of a biosensor are determined by these criteria in below chapter [5].

2.8.1 Sensitivity

This is thought to be the most crucial feature of a biosensor. The connection between the change in analyte concentration and the strength of the signal generated by the transducer is characterized as a biosensor's sensitivity. A biosensor should, in theory, create a signal in response to minor changes in the target analyte's concentration. Biosensors are needed to detect analytes in the ng/ml or fg/ml concentration levels, depending on the application. This is typically required for medical and environmental monitoring applications [5].

2.8.2 Selectivity

In the presence of other molecules or chemicals, this refers to the biosensor's capacity to selectively bind and react solely to the intended analyte. A false positive result occurs when a signal or reaction is created as result of interactions with an analyte that is not the target

analyte. This is typical in low-selectivity biosensors, which fail in clinical applications. Selectivity is particularly significant in medical applications, because the test sample or sample matrix, often blood or urine, includes large number of molecules that are highly similar like the target analyte and compete for binding to the biological receptor [5].

2.8.3 Stability

The biosensor's stability is critical, especially for biosensors that are utilized for continuous monitoring. This characteristic affects the biosensor device's capacity to maintain its function over time in the face of disruptions caused by external sources. Temperature, humidity, and other environmental factors can all be factors. Such disruptions have the potential to introduce inconsistencies in the output signal during measurement, compromising the biosensor device's precision and accuracy. This is because the biosensor device's transducers and other electrical components are largely temperature sensitive, and this can have a significant impact on their stability. Temperature can also alter the biological receptor's integrity, as this component degrades with temperature changes [5].

2.8.4 Detection limit

The lowest concentration of the target that can elicit a quantifiable signal or reaction is known as the detection limit. A biosensor's detection limit should be as low as possible. If it's going to be employed in medical applications, the target analyte may be present at extremely low quantities [5].

2.8.5 Response time

The time it takes for the biosensor to create a signal or response once the biological receptor interacts with the target analyte is determined by this attribute [5].

2.8.6 Range or linearity

The accuracy of the signal received in response to a set of samples with varying concentrations is determined by biosensor linearity. This property describes the biosensor's resolution, which is defined as the smallest change in the target analyte concentration that

will cause the biosensor to respond. Because most applications require a biosensor to assess a target analyte across a large concentration range, this is a critical feature [5].

2.8.7 Reproducibility

This is another crucial aspect in biosensing, and it relates to the biosensor device's capacity to produce same output signals or outcomes in multiple experimental runs. The biosensor's capacity to achieve these requirements is dependent on the transducer's ability to work in a precise and accurate manner [5].

2.9 Previous and Recent Projects of Biosensors

Previous recent projects, which used almost the different technique, software, technology, and equipment to produce and innovate the new project, were picked to generate a concept for improving and mitigating the disadvantages. Table 2.1 tabulates the previous recent studies on biosensor to detect urea .. These techologies will be explained in the this section. This section will be describing the summary of existing biosensors to detect Urea .

Table 2.1 Previous and Recent Projects of Biosensors

TITLE	DESCRIPTION	FINDINGS
Graphene-MoS2 SPR-based biosensor for urea detection (N. A. Jamil, N. B. Khairulazdan, P. S. Menon, A. R. Md Zain, A. A. Hamzah, and B. Y. Majlis) (2018)	The efficiency of graphene and MoS2 layers is considered in this article, which is based on Kretscmann arrangement [6].	The results show that urea sensitivity has improved. As a result, it is envisaged that this biosensor will be able to detect biomolecules more accurately [6].

An Extended Gate Field Effect Transistor-based (EGFET-based) Urea Microbiosensor Based on Polypyrrole (M. Oguz, I. Avci, and M. Sen) (2021)	The quantitative detection of urea in aqueous solution is described using an (EGFET) urea microsensor based on modified polypyrrole (PPy) [7].	The conductivity of the PPy was altered by different amounts of urea solutions. The EGFET-based urea microsensors might be used in a variety of portable applications, such as point-of-care diagnostics [7].
The Flexible Urea Biosensor Using Magnetic Nanoparticles (J.-C. Chou et al.)(2019)	Using electrochemical impedance spectroscopy and a voltage–time measuring system, the electrochemical impedance and response time of the urea sensor based on Magnetic Beads, Graphene Oxide, and Nickel Oxide were measured [8].	MBs/GO/NiO film had the lowest charge transfer resistance and good charge transition characteristics among the other sensors[8] .
LED-Based Portable Optical Biosensor for Measurement of Serum Urea Levels Using Urease Immobilized Agarose-Guar Gum Composite Film (C. Vaghela, M. Kulkarni, R. Aiyer, and M. Karve) (2018)	The LED light, optical fibre, and phototransistor used in the optical detection system provide a simple and portable measuring device [9] .	The urea biosensor has been successfully utilised to quantify normal and abnormal urea levels (pathological and non-pathological situations) in human blood samples with high accuracy. It provides a benefit for real-time sample analysis due to direct detection, which eliminates the need for pretreatment and allows for a very small sample volume [9].
The Analysis of Potentiometric Flexible Arrayed Urea Biosensor Modified by Graphene Oxide and γ-Fe2O3 Nanoparticles (Y.-H. Nien et al.) (2020)	Fabrication of urea biosensor based on urease-maghemite nanoparticles (γ -Fe2O3 NPs)/graphene oxide (GO)/nickel oxide (NiO) sensing membrane on silver conductive wire printed polyethylene terephthalate (PET) substrate using radio	The average sensitivity rose when the temperature was raised to 45 degrees Celsius. It also has great long-term storage stability and stability. The average sensitivity remained at 80.80% of the starting value after 29 days [10].

	frequency (RF) system and screen printing method [10].	
The Hysteresis Reduction Approach for Urea Biosensor Modified by Silver Nanoparticles (P.- Y. Kuo, Z.-X. Dong, and Y.-Y. Chen)(2021)	The purpose of this study is to diminish the hysteresis effect of a urea biosensor modified with a thin coating of silver nanoparticles (Ag NPs) and ruthenium dioxide (RuO2) [11].	The urea biosensor attained an average sensitivity of 48 mV/decade, linearity of 0.996, 0.37μM limit of detection (LDO), 22 seconds reaction time, and high selectivity, according to the experiment data [11].
Highly-Sensitive SPR Urea Biosensor Based on Urease Immobilized in Metal-Organic Zeolite Framework (L. Cheng, W. Zheng, L. Li, and Y. Zhang)(2021)	A multi-mode thincore multi-mode (MTM) surface plasmon resonance (SPR) structure with great sensitivity is presented and used in urea detection [11], [12].	The concentration of the urea solution may be determined by detecting the resonance wavelength value of the SPR spectrum, which is based on the functional connection between the resonance wavelength and the concentration of the urea solution. Fast reaction, great sensitivity, outstanding selectivity, and low cost are all advantages of the sensor [12].
The Stability Analysis of Potentiometric Urea Biosensor Under Microfluidic System and Remote Measurement (P.-Y. Kuo, Z.-X. Dong, and Y.-Y. Chen)(2021)	The stability of a potentiometric urea biosensor based on urease-Ag NPs/RuO2 sensing screen was investigated in this paper. The biosensor's reproducibility, repeatability, long-term measurement, and temperature effect were all investigated using the	The linearity and sensitivity of the remote measurement potentiometric urea biosensor were good [13].

	voltage–time (V–T) measuring technique [13].	
Investigation of Flexible Arrayed Urea Biosensor Based on Graphene Oxide/Nickel Oxide Films Modified by Au Nanoparticles (Y.-H. Nien et al.) (2020)	The flexible arrayed urea biosensor in this study is made up of silver paste electrodes that were screen printed [14].	Over a wide concentration range (0.01–100 mM), the flexible arrayed urea biosensor based on urease-Au NPs/GO/NiO sensing screen has good average sensitivity of 57.16 mV/decade and linearity of 0.998 [14].
Taguchi optimization of Surface Plasmon Resonance-Kretschmann biosensor using FDTD (N. A. Jamil, P. S. Menon, S. Shaari, M. A. Mohamed, and B. Y. Majlis)(2018)	The fullwidth-at-halfmaximum (FWHM) of the surface plasmon resonance (SPR) curve from a graphene-based SPR biosensor was optimised in this research [15].	The use of numerical analysis utilising Lumerical's FDTD and Taguchi's optimization analysis as an appropriate and reliable approach in improving the control factors of a graphene-based surface plasmon resonance (SPR) biosensor in order to obtain the best FWHM was highlighted in this study [15] .
Glass-based fluorescent immunobiosensor used for urea albumin fast detection (L.-C. Hung, Z.-Y. Lin, and Y.-N. Chou)(2021)	This effort aims to create a glass-based fluorescent immunosensing device for quick recombinant urine protein screening [16].	Regardless of the wealth divide or geographical issues, everyone may self-detect kidney illness and receive early identification, treatment, and recovery [16].
Urea Biosensor Based on a CO2 Microsensor (D. Fapyane, D. Berillo, J.-L. Marty, and N. P. Revsbech)(2020)	The urea biosensor is made up of urease immobilised in an alginate polymer, buffered at pH 6, and put in front of a newly designed rapid and sensitive CO2 microsensor with gas-permeable membrane shielding the electrodes [17].	With a simple CO2 removal pretreatment step, the urea biosensor was able to quantify urea in blood plasma [17].
Sweat-Based Noninvasive Skin-Patchable Urea	A urease immobilized photonic interpenetrating	Without the need of complex analytical tools,

Biosensors with Photonic Interpenetrating Polymer Network Films Integrated into PDMS Chips (S. Hussain and S. Park)(2020)	polymer network (IPNurease) film was used to create a wearable noninvasive biosensor for in situ urea detection and quantification [18].	the proposed PDMS biosensor chip provides a simple, easy, and cost-effective technique for urea detection [18].
Design and fabrication of a multimode optical fiber surface plasmon resonance urea biosensor (J. Li, J. Wan, M. Han, and H. Zhang) (2021)	A multimode optical fibre SPR urea biosensor was designed and built. Build a reflecting fibre optic sensor system as well. Varied thicknesses result in different levels of sensitivity [19].	With a simple CO2 removal pretreatment step, the urea biosensor was able to quantify urea in blood plasma [19].

2.10 Urea biosensor

Guibault et al. created the first urea biosensor in 1969. The investigation of this earlier urea biosensor was limited to its capacity to identify ammonium ions using a cation-selective glass electrode given by urease and directly proportional to urea concentration. There are two types of urea biosensors: enzymatic and nonenzymatic. Enzymatic and nonenzymatic biosensors each have their own set of benefits and drawbacks. Urea biosensors that use the urease enzyme hydrolyze the analyte urea into NH4 + and HCO3 ions. Figure 2.5 depicts the mechanism of the urease enzyme, which catalyses the hydrolysis of urea. The urea is measured following the creation of produced ions that cause a pH shift during the process. In reality, by utilising a separate transducer matched with the concentration of urea, it is simple to detect the ammonium ion (NH4+) in traces. By now, a number of urea electrodes have been created, many of which rely on ionresponsive field effect transistors, carbon nanotubes, and gold/silver/zincoxide/ironoxide based transducers. Improvements were made to the biosensor based on the enzyme coating, resulting in increased enzyme stability and decreased urea detection limits. Enzymatic biosensors, on the other hand, have limitations since they require expensive enzymes with short lives and high costs [20].

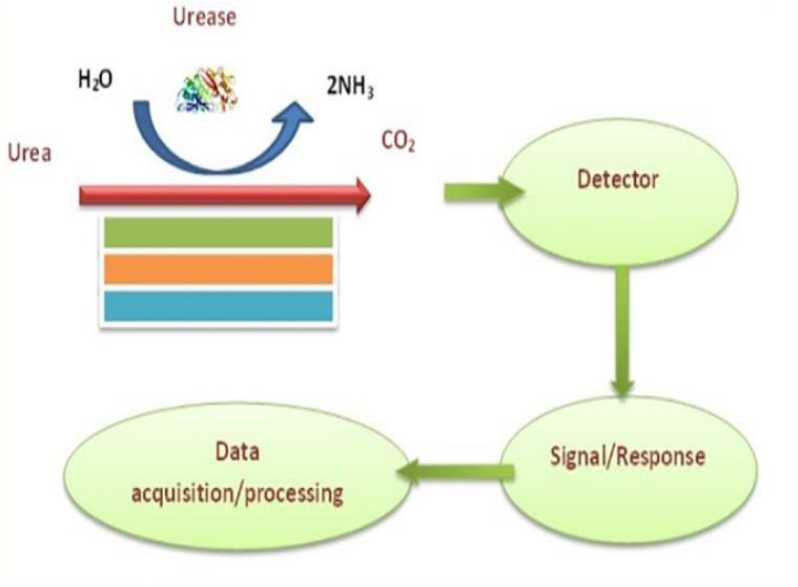

Figure 2.5 Schematic diagram of urea hydrolosis [20]**.**

Because biosensors are expensive, nonenzymatic biosensors that employ nanoscale bare and functionalized metals and metal oxides to substitute enzymes have been created.Nanosize bare and functionalized metals and metal oxides are attractive prospects for use in nonenzymatic biosensors because they are very sensitive and stable, in addition to cost reductions. Because of their wide range and high catalytic efficiency, they have been widely employed for the electrocatalytic oxidation of urea [20].

2.11 Classification of Urea biosensor

Other characteristics such as bioreceptors, transducers (kind of transduction element such as traditional/nanoorange material), and various sorts of physicochemical reactions may be utilised to determine the performance of different types of urea biosensors . Many examples of modern urea biosensors will be shown in below [20].

2.11.1 Potentiometric urea biosensor

An empirical approach for determining the potential difference between two electrodes is potentiometric measurement. This variation in potential differences is due to urea hydrolysis, and it might be recorded to provide quantitative urea assessment. After enzymatic hydrolysis of the analyte urea, the major product ammonium ion, carbon dioxide, ammonia gas, or pH

changed is formed in accordance with the urea concentration in the analyte. Many potentiometric urea biosensors are readily accessible and work on the medium pH shift principle; however, for pH-sensitive electrodes, the sensor reaction is heavily reliant on the sample solution's buffer capacity. For the quantitative detection of urea, a potentiometric urea biosensor based on very stable grafted fullerene was created. The urease enzyme was immobilised using fullerenes as a matrix. By using a post impregnation approach, a carboxylic group was grafted onto the surface of fullerene. In the presence of $(C_6H_{11}N)_2C$ and EDC hydrochloride, the urease enzyme formed a covalent bond with the carboxylic group of fullerene. Fourier transform infrared spectroscopy was used to validate the immobilisation process of the urease enzyme and the grafting of the carboxylic group (F.T.I.R.). On a screen-printed pH sensitive electrode, urease enzyme-based fullerene was deposited. For the quantitative measurement of urea, an acrylic membrane was placed on the electrode, which gives high stability and rapid reaction. The chemical process between modified fullerene and urease is depicted schematically in Figure 2.6 [20] .

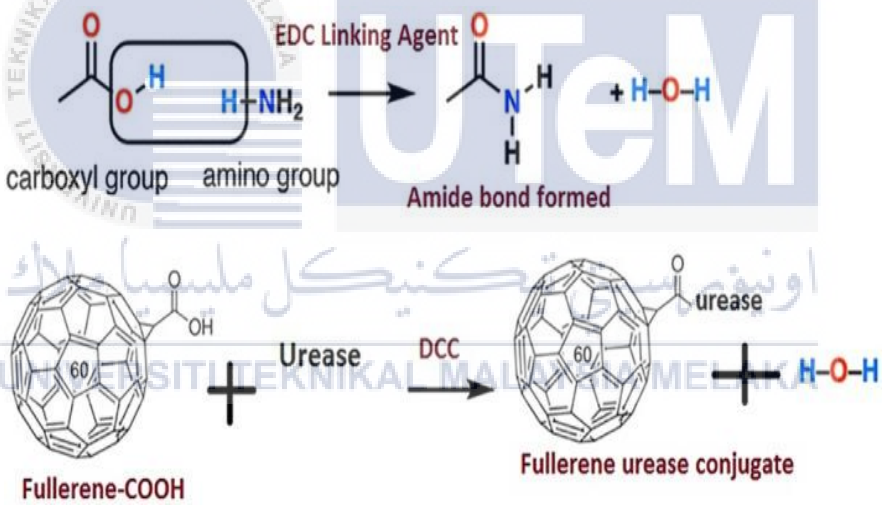

Figure 2.6 Schematic reaction mechanism between modified fullrene and urease enzyme [20].

The linear range of urea concentration for this potentiometric biosensor was 01.2–00.042 mM. To assess the urea level in the synthetic urine, a lab on a chip-based green urea biosensor was created. The electrochemical oxidation of ammonia produced from the Proteus vulgaris bacteria's surface membrane was used to measure urea. The optical lithography technology was utilised to make platinum electrodes and wholecell microbial sensors. Furthermore, P. vulgaris was employed on the surface of a platinum electrode to convert urea to ammonia, preventing obstruction on the platinum's surface as well as its

capacity to oxidise. The proposed study will serve as a platform for waste water sensing, tracking, in vivo urine, and point-of-care urea testing [20] .

2.11.2 Field effect transistor based urea biosensor

Field effect transistor-based biosensors are a promising tool in biological applications as semiconductor technology advances. The solid state reference system was compared to the transconductance compatible biosensors for differentiated read out electronics. The use of nafion as a supporting matrix allows for the production of reference field effect transistors (REFET) and enzyme field effect transistors (EnFET) as well as reduced primary load transition resistance. With urease immobilised, the biosensor membrane was placed in a conductive polymer-based matrix. By altering the photoresist/NafionTM, the device structure of polymer-based REFET and enzyme-based EnFET has been altered to give a differential pair transconductance curve with a large dynamic measuring scale. On a single chip, this system may be reproduced in tiny size . An ion selective field effect transistor dependent urea biosensor, similar to the potentiometric transducer, has been described. Zeolites of several sorts were synthesised (silicalite, nano beta zeolite, and zeolite L). The mucosal surface of the electrode was changed with a spin coater, and synthesised zeolites were placed directly to the modified electrode. Using a monolayer of several zeolite forms, the urease enzyme was adsorbed onto the ion selective field effect transistor. The proton-consuming urea cleavage process to NH_4^+ ions is required for urease biosensor function. A pH change occurs within the particular membrane as a result of this interaction, which is recorded by pH-sensitive field effect transistors. As a control, glutaraldehyde vapour was employed. Adsorption of enzymes on monolayers of silicalite and nanozeolite L has been demonstrated to result in a linear range increase of up to 01.50 mM. Figure 2.7 depicts an ion selective field effect transistor that was employed in the urea biosensor [20].

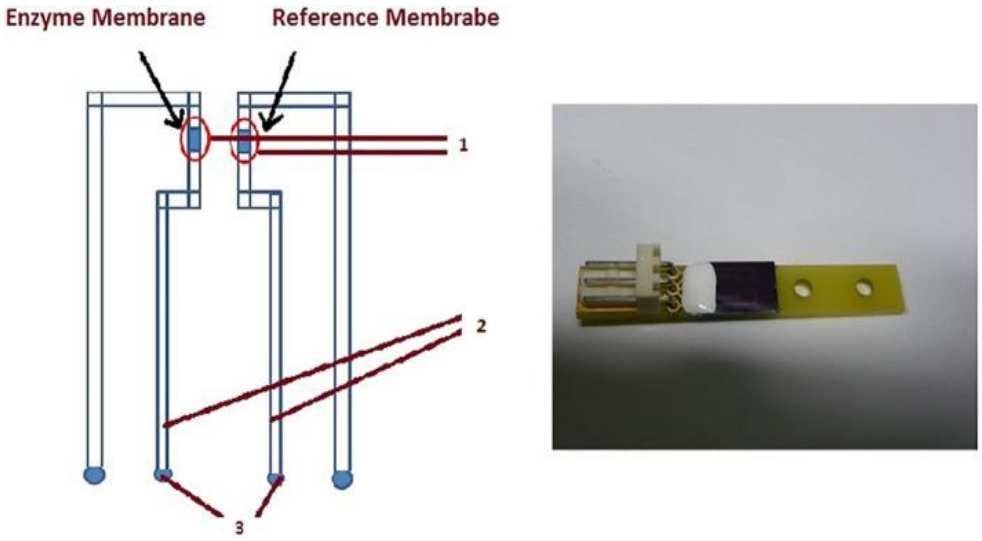

Figure 2.7 Schematic and general views of components of ISFET elements.1, gate areas; 2, p ± diffusion buses from source and drain of each transistor; 3, aluminium contacts [20]**.**

It has been discovered that using a monolayer of similar zeolites as a matrix for enzyme adsorption to manufacture potentiometric biosensors can result in an increase in linear range of activity, a decrease in the minimum urea determination cap, improved reproducibility and interreproducibility of the reaction, and a reduction in analysis time.Fenoy et al. devised a novel method for synthesising acetylcholine sensors and immobilising the enzyme Acetyl-cholinesterase on graphene-based field effect transistors. This approach included creating an electrical polymer layer with an amino moiety on a graphene channel. This copolymer base, poly (3-aminobenzylamine-co-aniline), not only provides a steady electrostatic charging state for urease immobilisation, but it also raises the pH (from 40.80 to 56.30 μA/pH unit). As a result, the developed biosensors had a limit of detection (LOD) of 2.3 μM and could track Ach in a flow configuration between 5 and 1000 μM. They also had a sensitivity of 26.6 0.7 μA/Ach decade and a relative standard deviation of 2.6 percent, indicating that the biosensor was highly reproducible [20].

2.11.3 Graphene-based urea biosensor

These sensors now have weak electrical conductivity, which has a significant impact on their sensing efficiency. Fibre grafting with different substances such as nitrogen, silver, zinc, and gold NPs resulted in a considerable improvement. Because of its intriguing physical urea biosensing capabilities, functionalised multilayered graphene (MLG) represents a novel innovation in several approaches. The MLG is produced using a simple,

safe, and repeatable procedure. It was made from MWCNTs that had been treated with concentrated H2SO3/HNO3 and then utilised to make urea biosensors. Functional MLG is a potential technique for urea biosensors, as well as a variety of other therapeutic bioanalytes . Because of its high catalytic activity in the oxygen reduction process, a nitrogen doped graphene-based urea biosensor has been created. Using a rotating disc electrode, the electrocatalytic property of a nitrogen doped graphene based urea biosensor towards the oxygen reduction process was determined. The detection limit and linear range of this graphene nanosensor were both excellent. Graphene fibre was used to create a photo electrochemical urea biosensor (PUB) with a broad linear range of 00.01 to 01500 micromolar and a very low detection limit of one nanomolar. Figure 2.8 shows a representation drawing of the stretchable PUB manufacturing technique and the recognition contrivance of its photoelectric reaction. Graphene oxide fibre was made by spinning graphene oxide (GO) dispersion via a special wet spinning machine with a congealing bath solution [20].

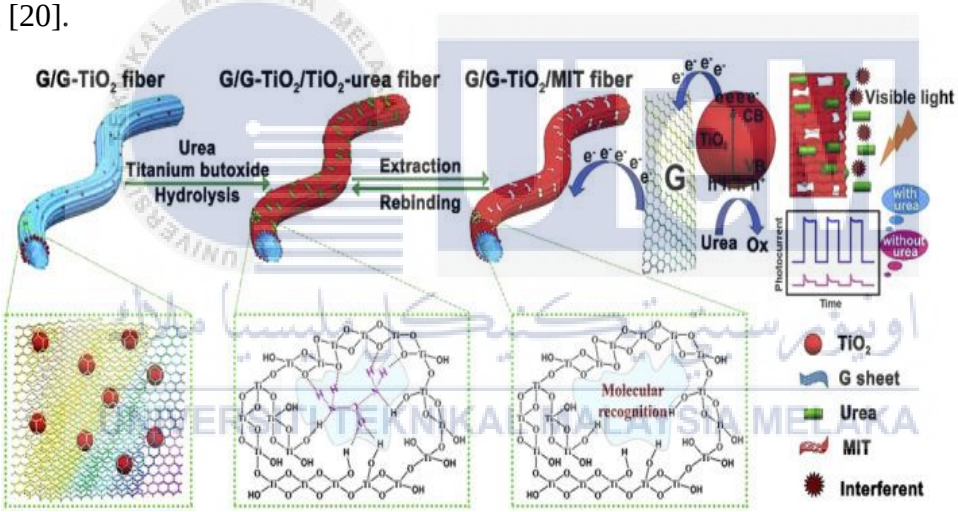

Figure 2.8 Graphene fibre based urea biosensor and its photo electrochemical detection process [20]**.**

2.11.4 Electrochemical urea biosensor

Electrochemical approaches were also investigated as a way to make urea detection in biosensors easier, more inexpensive, and more efficient. To detect the presence of urea in either the enzymatic or nonenzymatic form, redox processes can be monitored in electrochemical detection. By immobilising the urease on a gold electrode, a temperature-dependent urea sensor has been created. The hydrothermal method was used to create zeolite, and X-ray diffraction was used to establish its crystalline and amorphous nature. A gold

electrode was employed as a transducer, and synthesised zeolite was placed on the transducer surface using bovine serum albumin. The urease enzyme was subsequently immobilised on the modified electrode. The molar conductance catalytic activity of urea and urease was monitored using the cyclic voltammetry method. This urea biosensor made of zeolite demonstrated high stability and specificity. An amperometric polymer-based urea biosensor was developed to detect urea in blood and urine. An oxygenation functional group was electrochemically added to a pre-cleaned pencil form graphite electrode. A SNS aniline coated film was created using the aniline monomer. The DAFc was attached to the coated film using the amino group. Finally, the urease enzyme was bound to the DAFc's amino group. For urea detection, an Urease-DAFc- SNS aniline-based biosensing electrode was developed. The schematic illustration of the fabrication of a urease immobilised biosensor for urea detection is shown in Figure 2.9 [20].

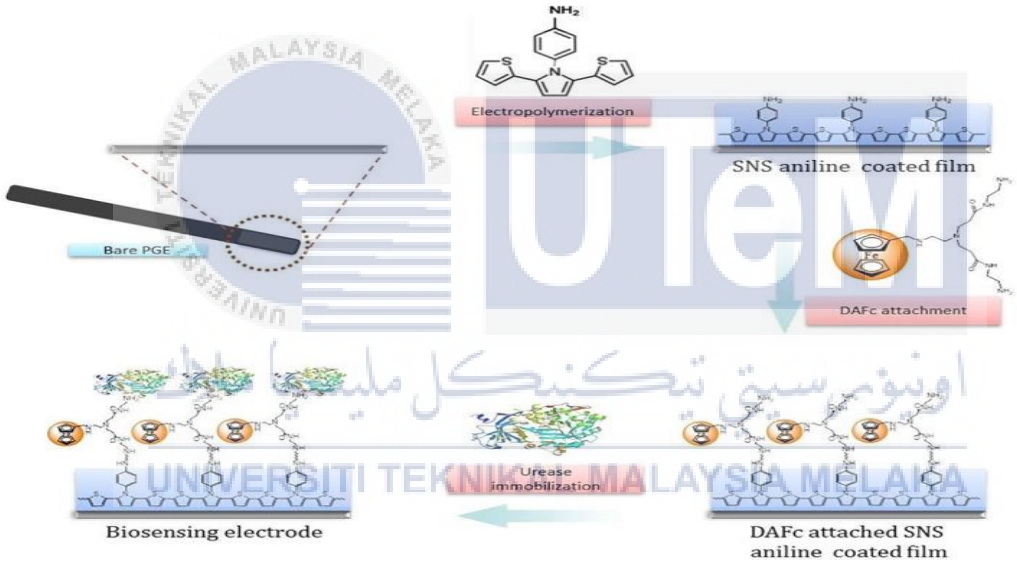

Figure 2.9 Schematic representation of preparation of urease immobilised biosensor electrode [20]

2.12 Electrodeposition

Electrodeposition has been practised for a very long time. By providing electrons to the ions in a solution, electrodeposition is a technique for depositing a thin layer of one metal on top of another metal to alter its surface properties. Current density, the kind of anions or cations in the solutions, bath composition and temperature, solution concentration, power supply current waveform, the presence of contaminants, and the physical and chemical makeup of the substrate surface are some of the variables that affect electrodeposition [21].There are several method to fabricate PPy/MWCNT nanofilm such as plasma [22] ,thermal [23] and sputtering [24] .

The plasma electrodeposition , due to their dependable energy storage capabilities and possible uses in wearable electronic devices, flexible and portable supercapacitors have been the subject of extensive research. Polypyrrole (PPy) was electrodeposited over He plasma etched carbon nanotube film (HCNTF) for electrodes of flexible supercapacitor with good performance due to the unique pseudocapacitance property of conducting polymer and the high conductivity and stability of carbon nanotube film (CNTF). He plasma etching can form amorphous carbon on the CNTF and increase its hydrophilicity, as shown by Raman spectra and contact angle measurements. This increased the electrodeposition of PPy onto the CNTFs and improved the adhesion between PPy and CNTF. The PPy/HCNTF electrodes and H3PO4/PVA electrolyte were used to create all-solid-state supercapacitors. Cyclic voltammetry tests showed that the capacitive performance of PPy/HCNTF is much higher than that of PPy/CNTF. The specific capacitance of the PPy/HCNTF supercapacitor determined by a galvanostatic charge-discharge method at 0.5 A g−1 is about 414 F g−1, which was maintained 92% after 5000 cycles, reflecting high cycle stability.

Moreover, the PPy/HCNTF supercapacitor could remain 96% of the original capacitance when it was bent for 500 times surrounding a cylinder with a diameter of 1.5 cm, showing perfect flexibility and great potential for flexible energy storage devices [22].The thermal electrodeposition can increased thermal conductivity using an electrodeposition process also. Some research were using copper/diamond composites were created. The cathode was at the bottom of the plating bath, and the electrodes were laid out horizontally. Diamond particles (10-230 m) were initially precipitated on the cathode substrate, and after copper was electrodeposited to fill the spaces left by the precipitated diamond particles, a Cu/diamond composite was created. Copper's deposition behaviour was

explored electrochemically, and estimates were made of the current densities of copper deposition under galvanostatic conditions. Unwanted hydrogen evolution resulted from the substrate with diamond particle layers having current densities that were 4–10 times greater than the substrate without diamond particle layers.

Potentiostatic conditions were used to create Cu/diamond composites without hydrogen evolution, and the resultant composites had compact morphologies. A specimen containing 49 vol% diamond particles with a mean diameter of 230 μm had the highest thermal conductivity of 600 W m−1 K−1, which is 1.5 times that of pure copper (ca. 400 W m−1 K−1) [23]. Among the most popular methods for depositing metallic thin films are electrodeposition and sputtering. Even when the chemical composition is held constant, the films produced by these processes often display diverse microstructures because they work according to different principles. Using electrodeposition and sputtering, films of $Fe_{70}Pd_{30}$ were created in this work with thicknesses ranging from 30 to 600 nm. The ammonia sulfosalicylic acid–based aqueous solution served as the source for the electrodeposited films, which were applied under a potentiostatic regime. In the meantime, a composite target deposited the sputtered films in the radio frequency regime.

Both methods have been shown to produce uniform, high-quality films. They have a distinct crystallographic structure, nevertheless. Despite the fact that every film was polycrystalline and Fe and Pd created a solid solution with a body-centered cubic structure, a palladium hydride was nevertheless synthesised. A palladium hydride phase was also found in the electrodeposited films, which were all polycrystalline and contained a solid solution of Fe and Pd with a body-centered cubic structure. This phase's occurrence caused internal tension in the films, which had an impact on their magnetic characteristics. In particular, the thickest electrodeposited $Fe_{70}Pd_{30}$ films showed out-of-plane magnetic anisotropy, whereas the magnetization easy axis lied in the film plane for all the sputtered films. By using magnetic force microscopy, the domain pattern of the electrodeposited films was examined. The outstanding quality of both the sputtered and electrodeposited films was further underlined by nanoindentation tests, with the former showing higher reduced Young's modulus and Berkovich hardness values [24].

2.13 Characterization

Fourier Transform Infrared Spectroscopy (FTIR), Scanning Electron Microscope (SEM), and X-Ray Diffraction (XRD) are three methods for determining whether a thin coating of one metal characteristic has been placed on top of another metal .

Scanning electron microscopes have opened up new fields of research in the fields of medicine and physical science since their invention in the early 1950s. Researchers are now able to analyse a far wider range of specimens thanks to the SEM. Compared to conventional microscopes, the scanning electron microscope has many benefits. The SEM's broad depth of field makes it possible to focus on more of a specimen at once. Since the SEM has a significantly better resolution, small specimens may be enlarged much more effectively. The SEM gives the researcher much greater control over the level of magnification because it doesn't use lenses but rather electromagnets. The scanning electron microscope is one of the most valuable tools in study today because of all of these benefits and the images' genuine remarkable clarity .

The major SEM parts are the electron source, the electromagnetic lens-enhanced column down which the electrons travel, the electron detector, the sample chamber, and the computer and display used to view the images. A focused beam of electrons is created by producing them at the top of the column, accelerating them as they descend, and passing them through a number of lenses and apertures. This focused beam of electrons then impacts the sample's surface. The sample is put on a stage in the chamber region, and a combination of pumps is used to evacuate both the chamber and the column (unless the microscope is built to function at low vacuums). The vacuum pressure will vary depending on how the microscope is built. Figure 2.10 shows the schematic of a scanning electron microscope [30].

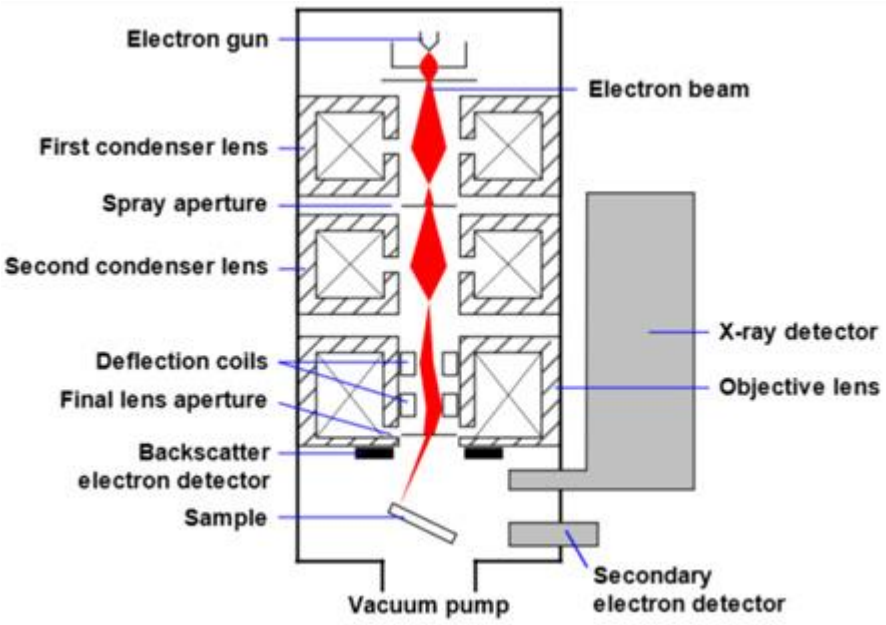

Figure 2.10 : **Schematic of a scanning electron microscope [30].**

Scan coils located above the objective lens are in charge of adjusting the position of the electron beam on the sample. These coils enable the beam to scan across the sample's surface. Information can be gathered about a specific location on the sample using this scanning. Several signals are generated as a result of the interaction between the electron and the sample. The right detectors then pick up these signals.

A high-energy electron beam is used to scan the sample in the scanning electron microscope (SEM) to create images. Secondary electrons, backscattered electrons, and distinctive X-rays are created as a result of the electrons' interactions with the material. One or more detectors gather these signals to create the visuals that are then shown on the computer screen. Depending on the accelerating voltage and the density of the sample, the electron beam penetrates the sample when it strikes the surface to a depth of a few microns. This interaction inside the sample results in the production of a variety of signals, including secondary electrons and X-rays .Figure 2.11 shows schematic of electron beam interaction [30].

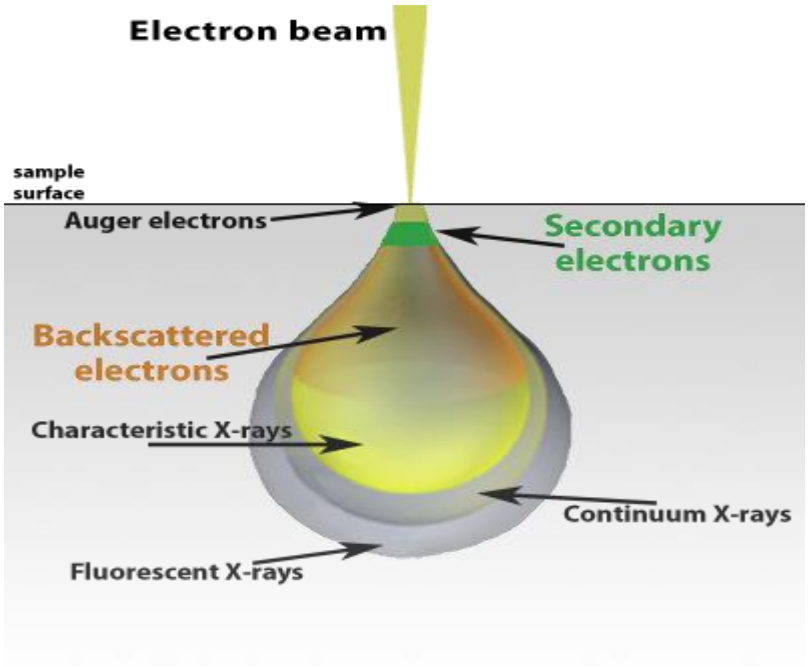

Figure 2.11 : **Schematic of electron beam interaction [31].**

The size of the electron spot and the volume of the electron beam's interaction with the sample are two variables that affect the greatest resolution that may be achieved in a SEM. Some SEMs can attain resolution below 1 nm, yet they cannot deliver atomic resolution. While desktop systems can offer a resolution of 20 nm or more, most recent full-sized SEMs typically offer resolution between 1 and 20 nm [35].

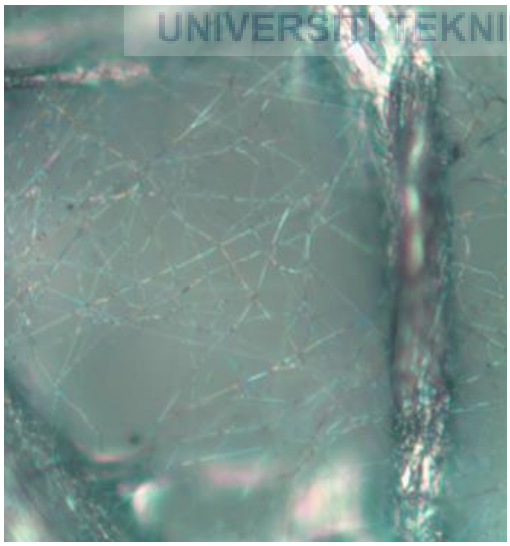

Figure 2.12 : **Optical microscope image of nanofibers [31].**

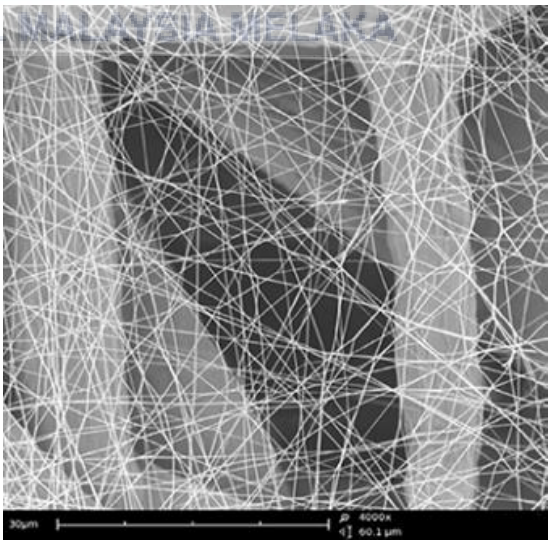

Figure 2.13 : Scanning electron microscope image at 4000x magnification of the same nanofibers [31].

Light microscopy is no longer able to characterise many structures due to the fact that materials and gadgets' dimensions are getting smaller. For instance, electron microscopy is needed to analyse the sample in order to ascertain the integrity of a nanofiber layer for filtering, as demonstrated in Figure 2.12 and 2.13 above [31] .

Next , FTIR stands for “Fourier Transform Infrared Spectroscopy” and it is the most common form of infrared spectroscopy.. All infrared spectroscopies operate under the premise that some IR energy is absorbed when it passes through a material. It is noted which radiation enters the sample. The spectra can be used to recognise and differentiate between molecules since different molecules, due to their various structures, emit various spectra. The spectra are virtually unique, much like a person's DNA or fingerprint. For a number of reasons, FTIR is the favoured approach to infrared spectroscopy. First off, the sample is not ruined. Second, it is far quicker than earlier methods. Thirdly, it is far more accurate and sensitive. Figure 2.14 shows A Schematic of a generic Michelson interferometer [32].

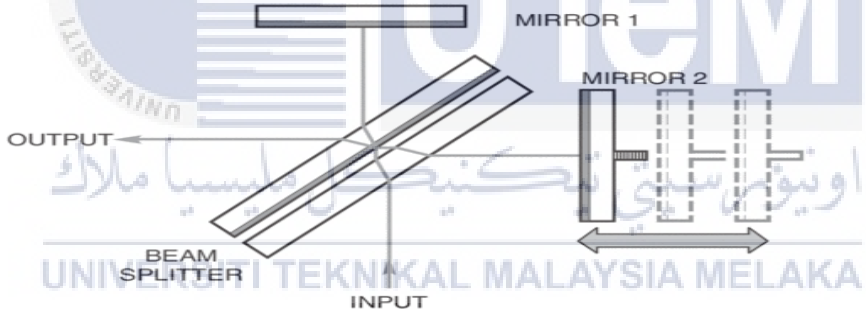

Figure 2.14 : **A Schematic of a generic Michelson interferometer [32].**

An FTIR is typically based on The Michelson Interferometer Experimental Setup . An example is shown in Figure 2.14 . A beam splitter, a mirror that is fixed (Mirror 1), and a mirror that accurately translates back and forth (Mirror 2) make up the interferometer. A unique substance that makes up the beam splitter transmits half of the energy that strikes it and reflects the other half. When it hits the beam splitter, radiation from the source splits into two beams. The beam splitter reflects the second beam back to the moving mirror while transmitting the first beam to the fixed mirror. The radiation is reflected back to the beam splitter by the stationary and mobile mirrors. Once more, at the beam splitter, half of this

reflected radiation is transmitted and half is reflected, causing one beam to travel to the detector and the other to return to the source. Figure 2.15 shows Overlay of the FTIR spectrum [33].

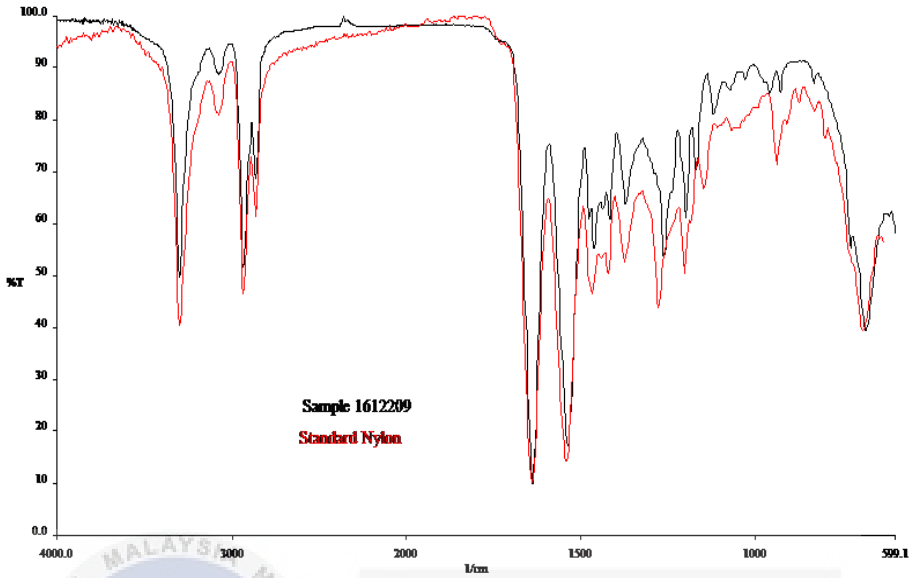

Figure 2.15 : Overlay of the FTIR spectrum with the best library search match of a standard Nylon [33].

The interpretation of data is not simple. The overall spectrum produced is fundamentally a series function of absorbed energy response. Only marginally distinct and degenerative, the absorbed bands shown in the spectrum. Other chemical and structural conditions can cause the specific "peak" of energy at a certain wavenumber to shift. Because of this, it cannot simply use a "look up" table to determine which band of energy a given waveform will unquestionably belong to. In order to accurately characterise the functionality displayed, the spectrum must be analysed as a full system, which likely calls for the most competent analysts in all of the spectrographic techniques [33].

When the chemistry is understood and standard reference materials are available, FTIR analysis, which is normally employed as a qualitative technique for material identification, can also be utilised as a quantitative tool to quantify particular functional groups. The amount of functionality present in the sample will be reflected in the absorbance's intensity. For instance, we characterise the amount of water in an oil sample and the level of oxidation and nitration using FTIR for quantitative analysis. It must be noted however that FTIR is a “bulk” analytical technique, in that little information can be gained

from trace or small concentrations of material in a sample (typically greater than 5% constituent) [33].

FTIR spectroscopy has a variety of uses, including monitoring processes, identifying molecules, and figuring out the constituents of a combination. The range of infrared wavelengths that a material absorbs is measured by FTIR analysis. This is achieved by exposing samples of a substance to infrared light (IR). The sample's capacity to absorb energy from infrared light at various wavelengths is examined to ascertain the molecular make-up and structure of the substance. The IR spectrum is searched against a large library of reference spectra to find unknown compounds. As long as it is possible to build a standard curve with known concentrations of the component of interest, materials can be quantified using the FTIR materials characterisation approach [33].

There are one more ways to ensure that a thin layer of one metal characteristic has been coated is present on top of another metal which is a typical method for figuring out a sample's composition or crystalline structure is X-ray diffraction. It can be used to ascertain the atomic structure of bigger crystals, including macromolecules and inorganic substances. It can determine sample composition, crystallinity, and phase purity if the crystal size is too tiny. Using this method, x-ray beams are passed through it. Instead of using much larger wavelengths, which would be unaffected by the spacing between atoms, X-ray beams are chosen because their wavelength is comparable to the spacing between atoms in the sample. This means that the angle of diffraction will be affected by the spacing of the atoms in the sample [34] .

Once inside the sample, the x-rays "bounce" off the atoms to change the direction of the beam at a different angle, theta, from the initial beam. This is the diffraction angle. Some of these diffracted beams cancel one another out, but positive interference happens if the beams have matching wavelengths. When two x-ray beams with the same wavelength that are whole number integers combine, a new beam with a higher amplitude is produced. This is known as constructive interference. For this particular angle of diffraction, the wave's increased amplitude results in a stronger signal. Then, using Bragg's law, $\sin \theta = n\lambda/2d$, where lambda is the wavelength added, theta is the angle of diffraction, and d is the separation between atomic planes, the angle of diffraction may be used to calculate the difference between atomic planes. The composition or crystalline structure can then be calculated from the spacing between atomic plates . Figure 2.16 shows Bragg's Law reflection [34].

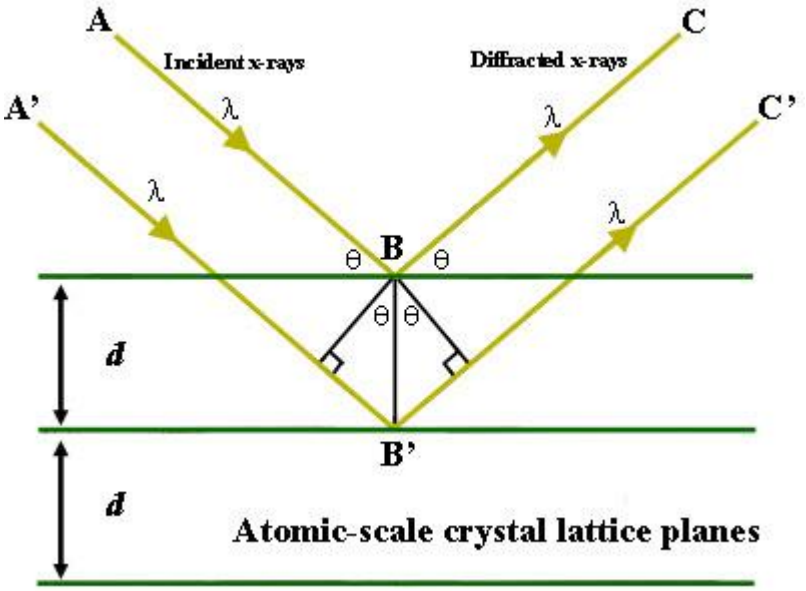

Figure 2.16 : **Bragg's Law reflection. The diffracted X-rays exhibit constructive interference when the distance between paths ABC and A'B'C' differs by an integer number of wavelengths (λ) [34].**

The result of X-ray diffraction plots the intensity of the signal for various angles of diffraction at their respective two theta positions. The two theta positions correspond to a certain spacing between the crystals or atoms in the samples, determined by the angle of diffraction from the incident x-ray beam sent into the sample. The intensity of the peaks is related to the amount of molecules in that phase or with that spacing. The greater the intensity of the peak, the greater the amount of crystals or molecules with that distinct spacing . Figure 2.17 shows X-ray diffraction plots of cubic silicon carbide [34].

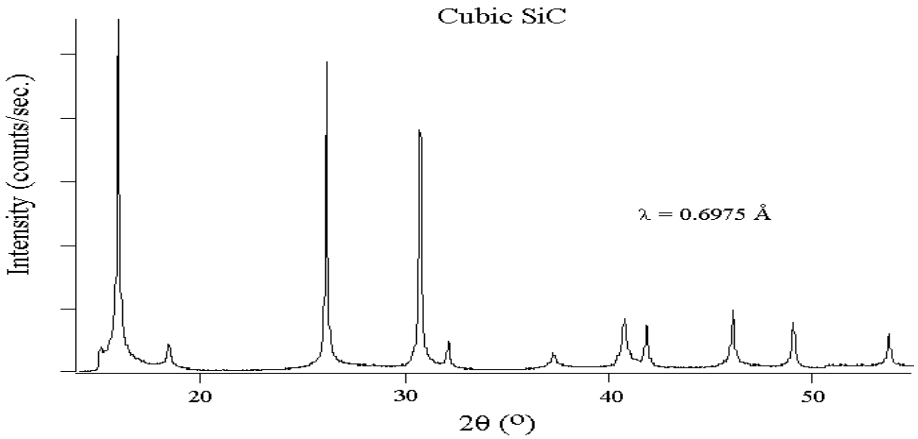

Figure 2.17 : **Figure X-ray diffraction plots of cubic silicon carbide [34].**

Peak width and crystal size have an inverse relationship. A larger crystal is associated with a thinner apex. The presence of a smaller crystal, a flaw in the crystalline structure, or an amorphous solid, which lacks perfect crystallinity, is indicated by a wider peak. The patterns identified by XRD analysis can be utilised to identify a sample's composition for smaller samples. The diffraction patterns for elements, compounds, and minerals are stored in a huge database of these substances. When the pattern for an unknown compound matches the position, width, and relative heights of the diffraction patterns, the element's identity can be confirmed by comparing it to values from the literature and experiments [34].

2.14 Comparative study conclusion

A brief research on efficient urea biosensor production and use has been given. During the review, all of the components involved in producing a biosensor were carefully considered, including the kind of material/nanomaterial, matrix/substrate, enzymatic/nonenzymatic, immobilization/binding procedure, and transduction mechanisms. The comparative output characteristics of the individual urea biosensors were presented in Table 1 for a simplified presentation.

Table 2.2 Comparative study of all urea biosensor

Material Used	Method of urease immobilisation	Linear range	Detection limit	Response time	Sensitivity	Reference
Fullerene (potentiometric)	Covalent	2.31 × 10−3 M to 8.28 × 10−5 M.	0.1 mM	_	59.67±0.91 mV/decade	[25]
Urease nanoparticle (potentiometric)	Immolilisation by glutarid acid	2 to 8.0 µM/L	1µM/L	10s	23mV/decade	[26]
Graphene (FET)	Electrostatic	5 to 1000 µM	2.3µM	130s	-26.6mV/decade± µA/Ach decade	[27]
Graphene fibre (photo electrochemical)	-	0.01 to 1500 µM	1 nM	-	high	[28]
Ferrocene (Electrochemical)	Crosslinked by glutaradehyde	0.12 to 8.5 mM	12 µM	2s	0.54µA/mM	[29]

2.15 Application of biosensor

The samples must be submitted to a laboratory for testing in traditional 'off-site' analysis. These procedures provide the best quantification accuracy and lowest detection limits, but they are costly, time-consuming, and need highly skilled workers. Because of the aforementioned limitations, biosensor technology has sparked many attention. In recent years, the area of biosensor development has seen tremendous expansion, with new applications in a wide range of fields. As shown in Figure 2.10, they include environmental monitoring, illness detection, food safety, defence, medication discovery, and many others. Below is an overview of the few and selected representations, as well as samples of developed biosensor applications [5].

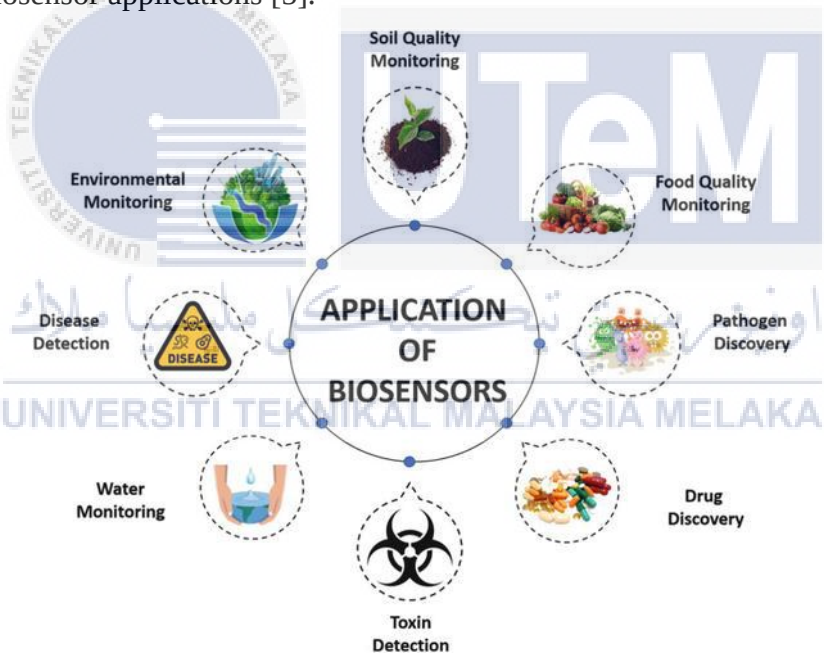

Figure 2.18 : Applications of Biosensor [5]**.**

2.15.1 Environtment

Pollution gives effect on human health and, as a result, can reduce one's quality of life. For quantitative and qualitative determination of target analytes, sensitive and selective techniques are required, depending on the goal. Chemical agents, organic pollutants, potentially poisonous substances, and infections that may represent a health threat have all been detected using biosensors in environmental monitoring [5].

2.15.2 Food Sector

Biosensors are frequently used in the food industry for quality control and assurance. Biosensors have been used as on-line or at-line quality sensors in the production process, allowing for quality sorting, automation, and cost and time savings. Biosensors have also been developed to detect certain ingredients in food. These devices detect chemicals or biological substances that can taint food or alert users to the presence of unwanted materials [5].

2.15.3 Medical

The majority of biosensors described in recent years have been discovered to be based on molecular interactions, which are generally used in various ways at various sizes. Biosensor applications are fast expanding in the field of medical science. Because of the disease's widespread frequency, high mortality rate, and recurrence after therapy, cancer diagnosis and treatment are of significant interest. Biosensors can be used in medicine to monitor diabetic blood urea levels, identify infections, and diagnose and track cancer growth. Early identification of cancer and successful therapy delivery might be aided by the use of developing biosensor technologies. Biosensors may identify the existence of a tumour, whether benign or malignant, by measuring the amounts of particular proteins produced and/or released by tumour cells. They can also determine whether or not a treatment is effective in reducing or eliminating malignant cells. Biosensors are now being used to detect cardiac signs and give early diagnosis as a consequence. Because biosensors are based on electrical measurements and also incorporate biological molecular recognition components to achieve desired selectivity with a specific biomarker of interest, they have been demonstrated to offer substantial advantages over standard diagnostic techniques [5].

2.16 Summary

At the end of this chapter, in various research project comparison on technologies, method, different technique, software, technology, and equipment that have been discussed, it is simpler to approaches the best outcome of the project. The outcome of examining previous researchers' study has a positive impact on this project since the right and appropriate approach will be used while keeping the weak point in mind. After reading their research, I want to utilise more on making the a finer nanoelectronic biosensor for detecting urea.

CHAPTER 3

METHODOLOGY

3.1 Lists of equipment

This section will explain the device and materials that used in this small-scale of project. The potentiostat will do the electrodeposition process of the electrodes and the Comsol Multiphysics software is used to simulate sensogram results to get the targeted redox.

Table 3.1 List of equipments

Equipment	Quantities
Potentiostat	1
Nova 2.0	1
Carbon plate	1 (1cm x 2cm)
Aluminium plate	1 (1cm x 2cm)
Copper plate	1 (1cm x 2cm)
Stainless steel plate	1 (1cm x 2cm)
Hand notcher	1
Foot shear	1
Bandsaw Machine	1
X-Ray Diffraction Machine	1
Scanning Electron Microscope	1
Fourier Transform Infrared Spectroscopy	1

3.1.1 Potentiostat

In a multiple electrode electrochemical cell, a potentiostat is an analytical device that regulates the potential of the working electrode. The potentiostat is made up of several internal circuits that allow it to work. Potentials and currents are created and measured by the circuits. The electrodes of the electrochemical cell are connected to the potentiostat circuit through external cables and a cell cable. The cell cable connects the working, counter (auxiliary), and reference electrodes on one end and the potentiostat cell cable connection

on the other end of a standard three-electrode cell. The applied signal is controlled by the potentiostat's internal circuitry. In potential controlled approaches, for example, the working electrode's potential is maintained in relation to the reference electrode. At the same time, current flows between the working and counter electrodes. Only a minimal amount of current may travel between the working electrode and the high impedance reference electrode thanks to the potentiostat circuit. While contemporary potentiostats are more complicated than this page can describe, it will provide a fundamental review of potentiostat circuitry to help to understand how they work [35].

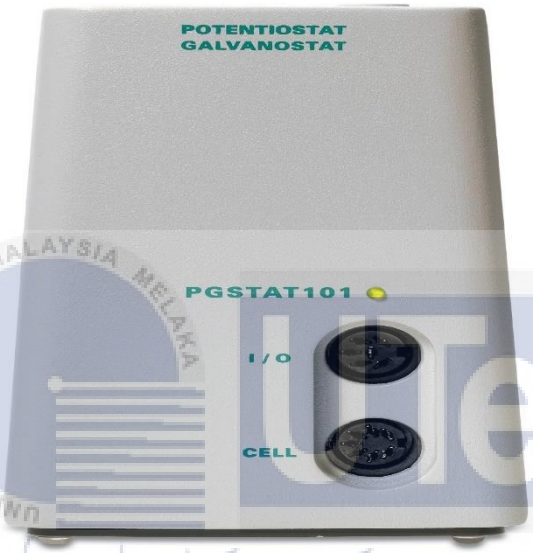

Figure 3.1 Potentiostat

3.1.2 NOVA 2.0 – Advance Electrochemistry Software

Metrohm Autolab's new electrochemistry programme is NOVA 2.0. This programme is used to control all Autolab equipment and accessories that are compatible.NOVA, designed by electrochemists for electrochemists, incorporates over two decades of user experience and the latest.NET software technology to give your Autolab potentiostat/galvanostat additional power and versatility.NOVA 2.0 combines the previous versions' capability and flexibility with a simple and modern user interface. NOVA's design is built on simple and effective graphical representations of common activities that the instrument may do. This

intuitive and straightforward UI offers a basic user experience. Both novice and seasoned users will quickly feel at ease with the software [36].

Figure 3.2 Advance Electrochemistry Software

3.1.3 Carbon plate

Carbon plates also known as graphite plates that have been extruded and isostatically pressed. Carbon plates are strong, brittle, high-temperature resistant, electrically conducting, and self-lubricating. Carbon atoms are arranged in layers in graphite Graphite is a substance that is black, glossy, and opaque. It's not transparent. The carbon layers easily slide onto paper, leaving a black impression, which is why they're used in pencil leads. Water does not dissolve graphite. It has a high melting point and is an excellent electrical conductor, making it an excellent material for electrolysis electrodes. Because these delocalized electrons may all travel in the same direction, graphite is an excellent electrical conductor [37].

Figure 3.3 Carbon plate

3.1.4 Aluminium plate

Aluminium plate is created by forcing metal through high-pressure rollers into a thinner, longer form, a surprisingly simple process that is also used to make aluminium sheet and aluminium foil. Aluminium has a high conductivity, is simple to fabricate, and is relatively affordable. Surface oxidation (anodization), which stops current flow, is the limit for electrodes. At room temperature, aluminium metal reacts easily with water to generate aluminium hydroxide and hydrogen. The reaction doesn't usually happen because the raw metal is naturally coated with aluminium oxide, which prevents it from coming into direct contact with water [38].

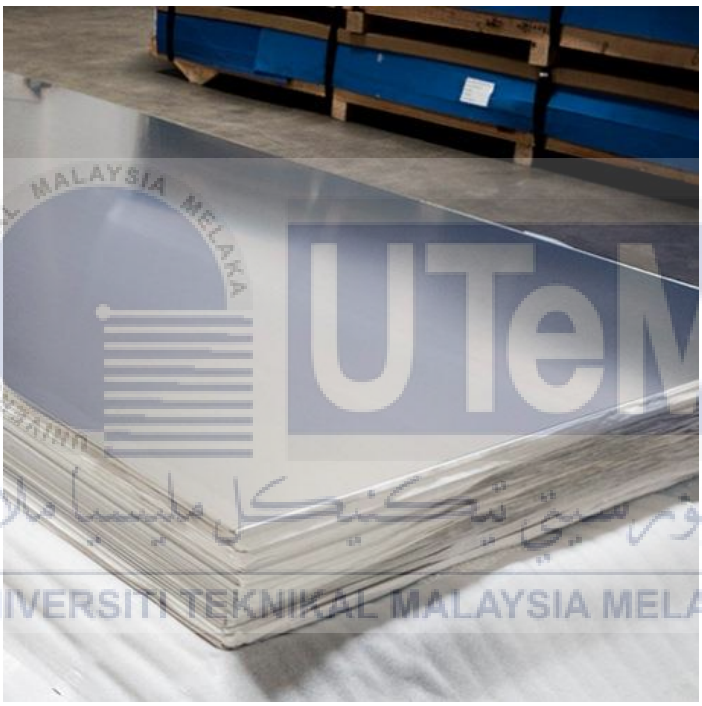

Figure 3.4 Aluminium plate

3.1.5 Copper plate

Copper is a simple to work metal that is a good heat and electrical conductor. Its ductile and malleable properties, as well as exceptional thermal and electrical conductivity and corrosion resistance, make it ideal for use in components.This copper sheet can be used as an electroplating sacrificial anode. This electrode will provide pure copper content in the solution when employed as a sacrificial anode. On the cathode side, a steady and persistent

metal deposition is ensured. Suitable for all galvanic plating applications requiring extreme purity [39].

Figure 3.5 Copper plate

3.1.6 Stainless steel plate

Stainless steel is a category of iron-based alloys with a minimum 11 percent chromium, a composition that prevents from rusting while also providing heat resistance. Stainless steel is also visually beautiful, easy to care for, durable, and offers a variety of elements in addition to environmental benefits [40].

Figure 3.6 Stainless steel plate

3.1.7 Hand Notcher

This piece of machinery is a hand-operated corner notcher that is used to make pans and boxes. It cuts notches at 90 degrees to make bending flat sheets into a box or pan easier [41].

Figure 3.7 Hand Notcher

3.1.8 Foot shear

These manually operated squaring shears, also known as foot shears, kick shears, or stomp shears, are the most cost-effective way to correctly cut big sheets of sheet metal. This diverse collection may be used to cut steel , aluminium, stainless steel, and other metal materials [42].

Figure 3.8 Foot shear

3.1.9 Bandsaw machine

A bandsaw is a power saw that uses a long, sharp blade formed of a continuous band of toothed metal stretched between two or more wheels to cut material. Although they can cut a variety of materials, they are typically used in woodworking, metallurgy, and lumbering [43].

Figure 3.9 Bandsaw Machine

3.2 System Operation

This project firstly need to do the electrodeposition of the electrode which is copper, carbon, stainless steel, and aluminium by coating the the electrodes in PPY(polypyrrole)/MWCNT(multi-walled carbon nanotube) solutions. Electrodeposition is a method of creating solid materials from a solution of molecules, ions, or complexes. The ultimate result will be better if the electrodeposition procedure is delayed.So, after coating the electrodes it need to leave and stay in the solution at least for 5 to 10 seconds to see a better results .After coated the electrode in PPY/MWCNT solutions it need to be put in Methanol solutions . The characterization will be using SEM (scanning electron microscope) A beam of focussed electrons of relatively low energy will be used to study the deposited film morphology and will scans a focused stream of electrons over a surface to create an image . The XRD (X-ray diffraction) helps find the geometry or shape of a molecule using X-rays and can makes it easier to check the AI material of the elctrodes. The FTIR will check composition functional group . After that the relationship between voltage current and the

surface area of the electrode needs to be analyzed. The immobilization will the gives rise to an efficient and simple biosensor.After dropping the urea solutions with certain molarity on the electrode , measure the sensitivity of the biosensor using the Comsol Mutiphysics software to check the sensogram results to get the targeted redox . Figure 3.10 below shos the flochart of urea biosensor fabrication.

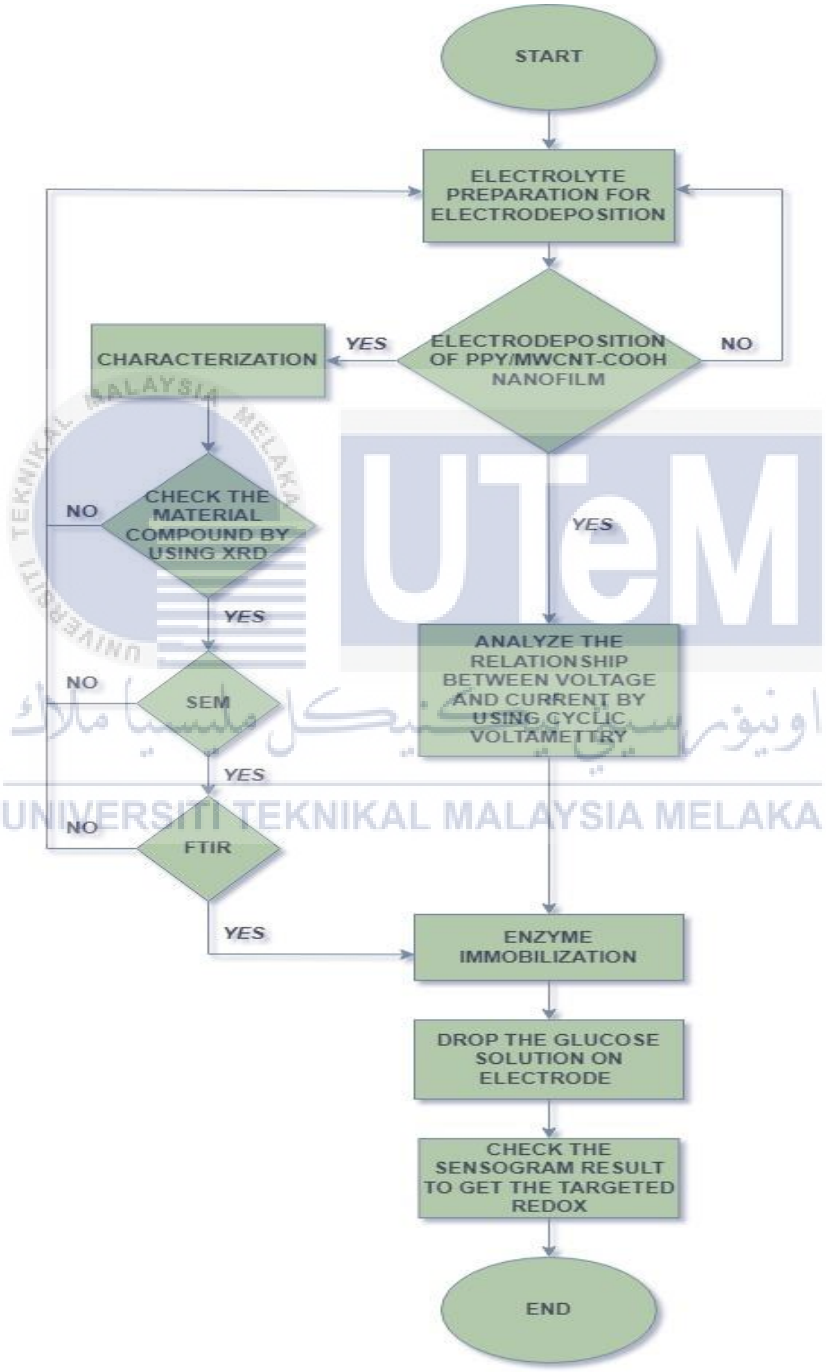

Figure 3.10 Flow chart of urea biosensor fabrication

3.3 Different Material Process for Electrode

3.3.1Copper Plate

Figure 3.11 shows the cutting of the copper plate using Hand Notcher by each length which is 2 cm

Figure 3.11 Cutting of the copper plate using Hand Notcher

Figure 3.12 is the process of the copper plate that has been cutted using foot shear after has been marked

Figure 3.12 Cutting the copper plate using Foot Shear

Figure 3.13 shows the copper plate that has been cut that each of their width of the copper is 2cm .

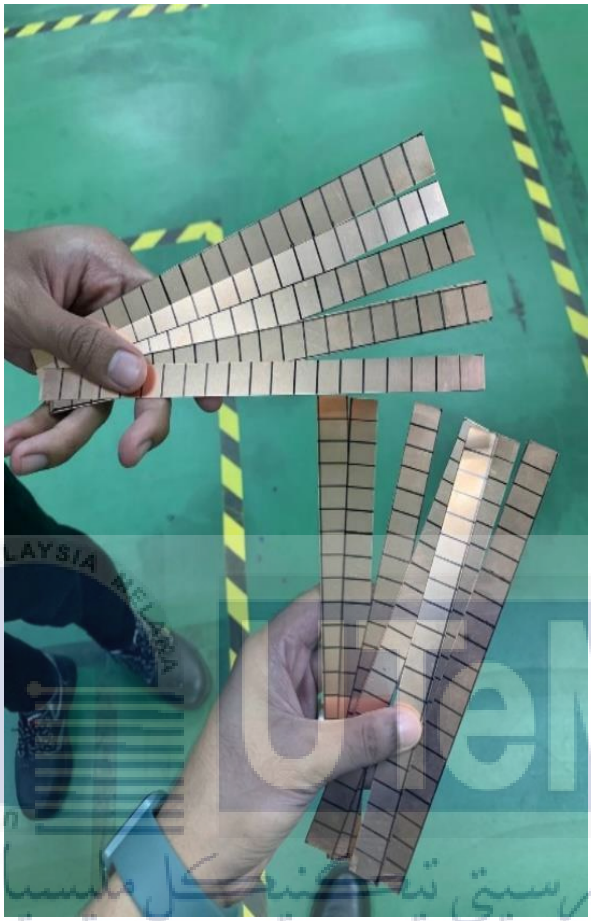

Figure 3.13 Copper plate after cutted using Foot Shear

3.3.2 Aluminium Plate

Figure 3.14 shows the cutting process of the aluminium plate by using Bandsaw machine . We cut in 1cm in width and 2 cm in length

Figure 3.14 Cutting the aluminium plate by using Bandsaw Machine

The rusty part will be removed by cleaning the plate as shown in Figure 3.15

Figure 3.15 Cleaning the rusty aluminium plate by using sponge and soap

3.3.3 Stainless Steel Plate

Figure 3.16 shows the stainless steel plate that has been marked while figure 3.17 shows the cutting process after has been marked . We cut in 1cm in width and 2 cm in length .

Figure 3.16 Marked the stainless steel

Figure 3.17 Cutting process of the stainless steel

3.3.4 Carbon plate

Figure 3.18 shows the carbon plate that has been marked while figure 4.11 shows the cutting of the carbon plate process after has been marked . We cut in 1cm in width and 2 cm in length .

Figure 3.18 Marked the Carbon plate

Figure 3.19 Cutting the carbon plate

3.4 PPY/MWCNT coating on electrode

3.4.1 Making MWCNT solution

These are the materials that have been used for making PPy/MWCNT solution. As shows at figure below, Figure 3.20 shows the 50ml deionized water in the beaker. After that, Figure 3.21 shows the MWCNT (multi-walled carbon nanotubes) powder. Then, Figure 3.22 shows the SDBS measurement by using Weighing Digital Scale. Besides that, Figure 3.23 shows the MWCNT measurement by using Weighing Digital Scale. Finally, Figure 3.24 shows the MWCNT and SDBS being put into Deionized Water.

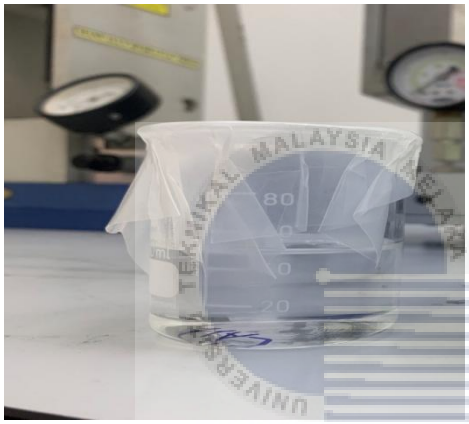

Figure 3.20: Deionized Water

Figure 3.21 Multi-walled Carbon Nanotubes

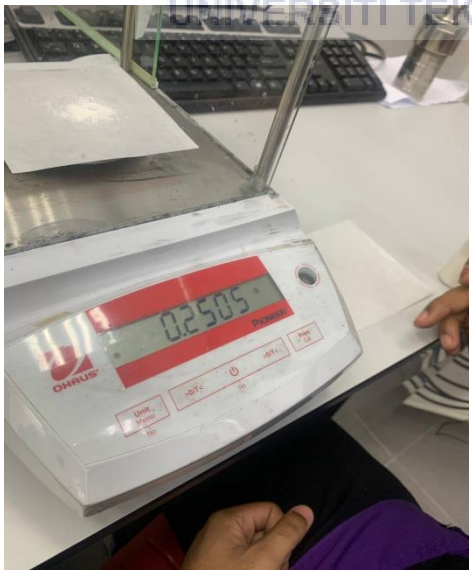

Figure 3.22 Measuring SDBS around 250 mg

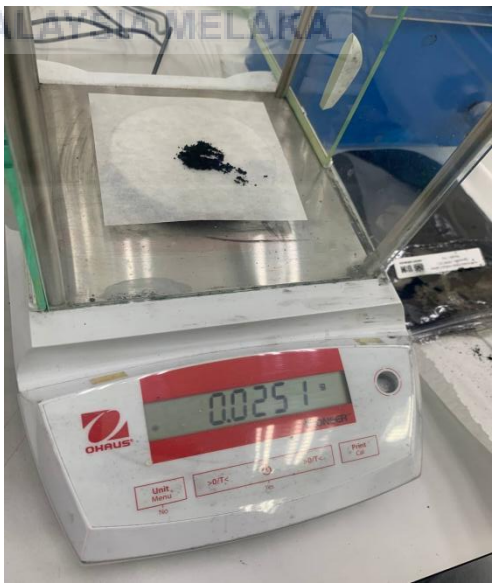

Figure 3.23 Measuring MWCNT around 25 mg

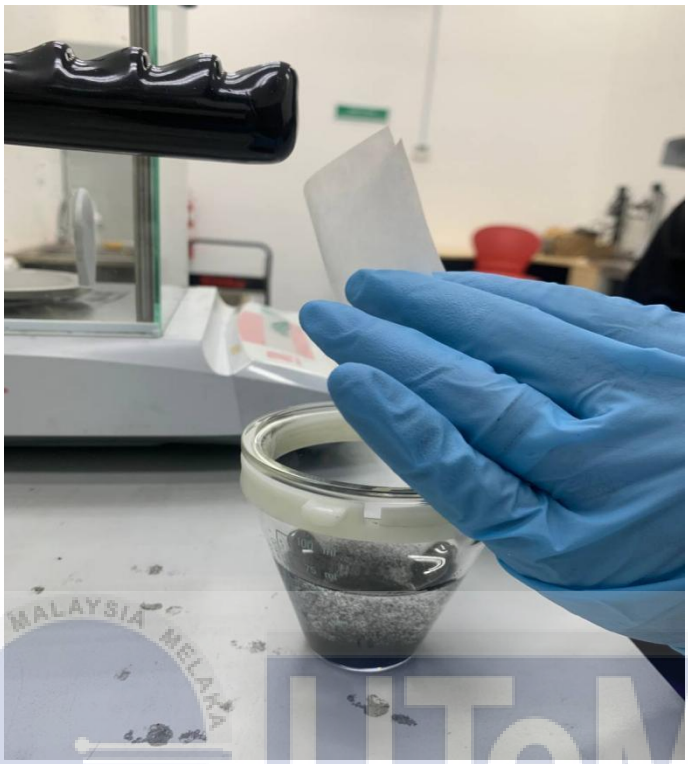

Figure 3.24 : Inserting SDBS and MWCNT into Deionized Water

3.4.2 Sonification Process

After making the SDBS and MWCNT solution, the proceed to sonicate the solution by using Ultrasonic Cleaner for 4 hours. Figure 3.25 shows the sonication process.

Figure 3.25 : Sonicating the MWCNT solution for 4 hours

3.4.3 Electrodeposition Process

After sonicate the SDBS/MWCNT solution for 4 hours, Plypyrrole (PPy) is added to the solution. As shown at Figure 3.26 and 3.27, Polypyrrole (PPy) been added to the SDBS/ MWCNT solution. At Figure 3.28, the new solution which is PPY/MWCNT is being stir by using Magnetic Stirrer for 5 minutes. Lastly, Figure 3.29 shows the Electrodeposition process.

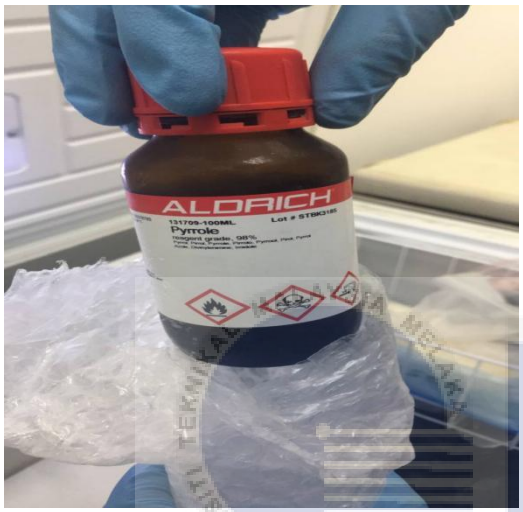

Figure 3.26: Polypyrrole

Figure 3.27: Putting Polypyrrole into MWCNT solution

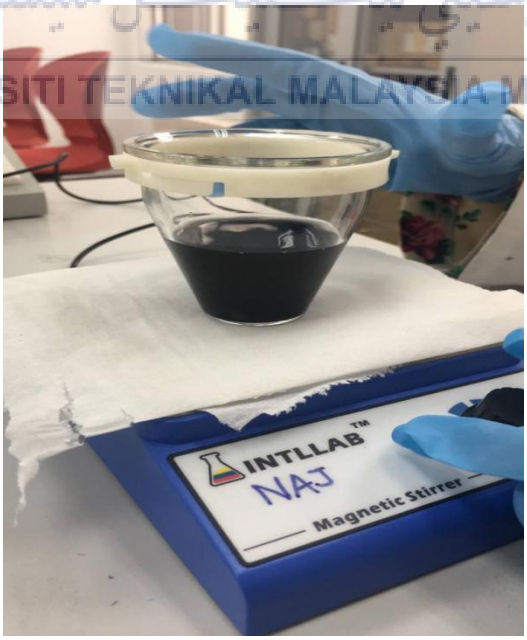

Figure 3.28: Stir the PPY/MWCNTM solution using Magnetic Stirrer

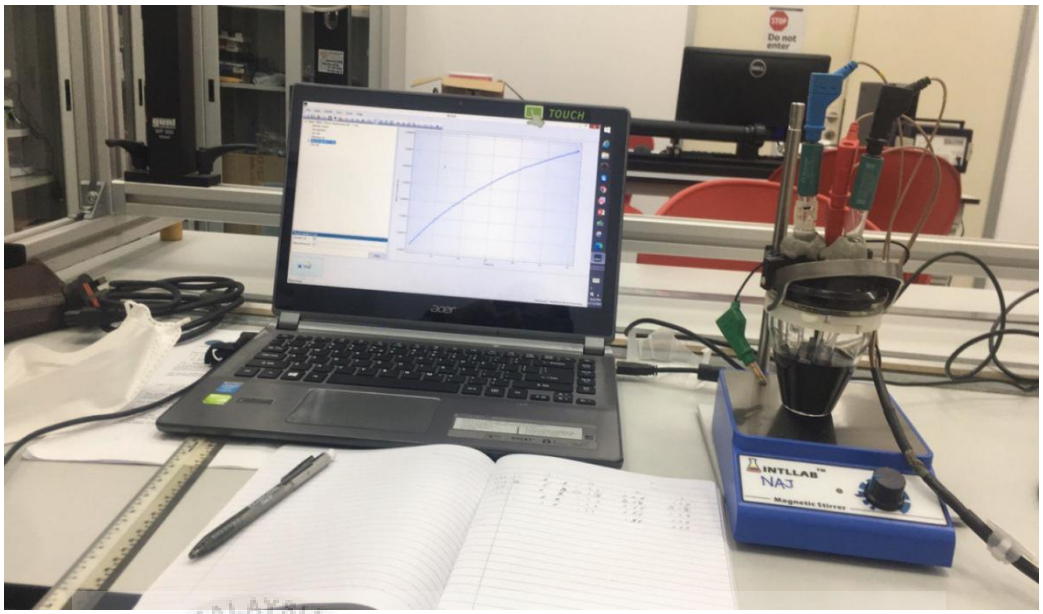

Figure 3.29 : Electrodeposition process of PPY/MWCNT solution on electrode

3.5 Procedure Cyclic Voltammetry in PBS (Phosphate Buffered Saline) solution

3.5.1 Dissolve PBS tablet in Deionized Water

Figure 3.30 shows that the PBS (Phosphate Buffered Saline) that is going to be added into Deionized Water at Figure 3.31. The ratio of the PBS tablets and Deionized (DI) water is 1:100ml as shown at Figure 3.32

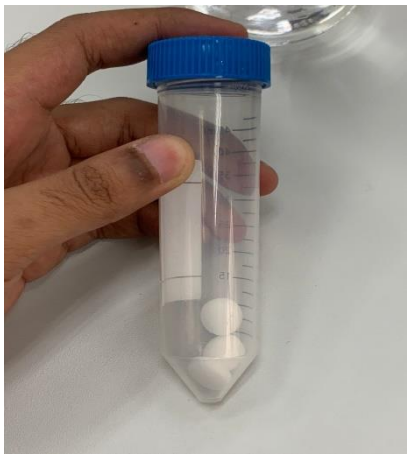

Figure 3.30 : **PBS tablets**

Figure 3.31: Deionized (DI) Water

Figure 3.32 : Dissolving PBS into 100 ml Deionized Water

3.5.2 Cyclic Voltammetry of different electrode in PBS solution

After making the PBS solution, proceed to the cyclic voltammetry process. Figure 3.33 shows the PBS cyclic voltammetry method with different electrodes.

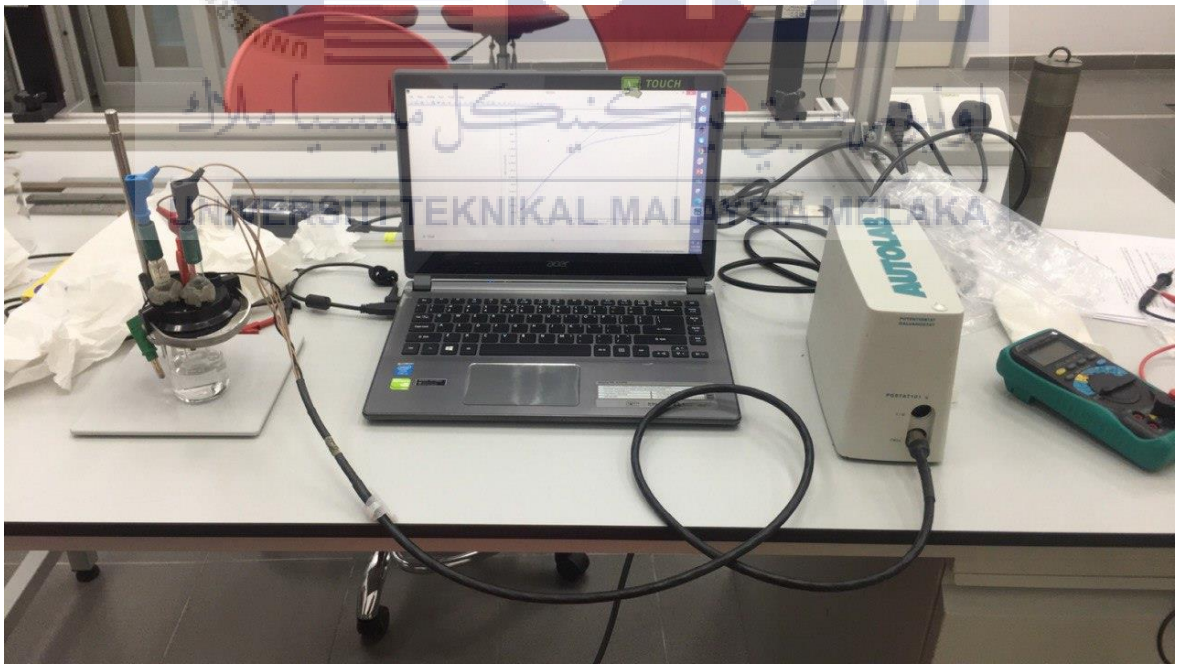

Figure 3.33 : Cyclic Voltammetry process PBS of different electrode in PBS solution

3.6 X-Ray Diffraction Machine (XRD)

The technique of X-ray diffraction analysis (XRD) is used in materials research to identify a material's crystallographic structure. XRD works by exposing a material to incoming X-rays and then measuring the intensities and scattering angles of the X-rays that escape. Figure 3.34 shows the XRD Machine that have been used for this project. Figure 3.35 shows the sample that have been delivered for XRD checking.

Figure 3.34: XRD Machine located at Fakulti Kejuruteraan Pembuatan (FKP), UTeM.

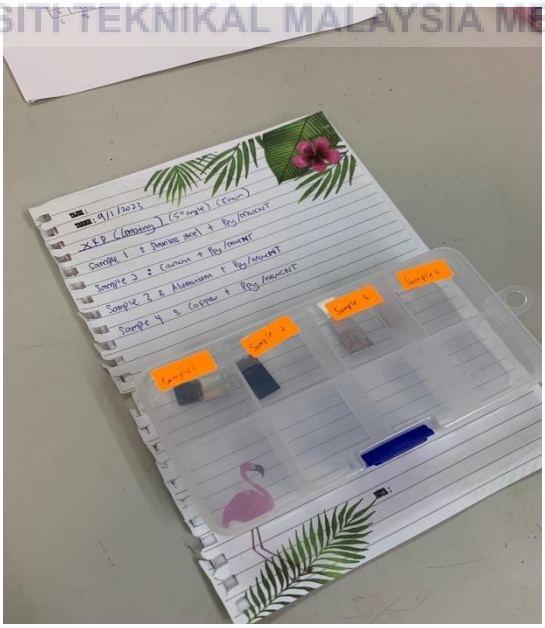

Figure 3.35 : Sample delivering for XRD machine.

3.7 Scanning Electron Microscope (SEM)

The scanning electron microscope (SEM) is a tool that creates an image using electrons rather than light, significantly enlarging it. At the top of the microscope, an electron beam is generated by an electron cannon. The vacuum-sealed microscope is traversed by the electron beam vertically. Through the passage of electromagnetic fields and lenses, the beam is narrowed down and directed toward the sample. Electrons and X-rays are released when the beam hits the sample. Figures 3.36 and 3.37 depict the SEM machine that was utilised for this project as well as the sample that was provided for SEM inspection.

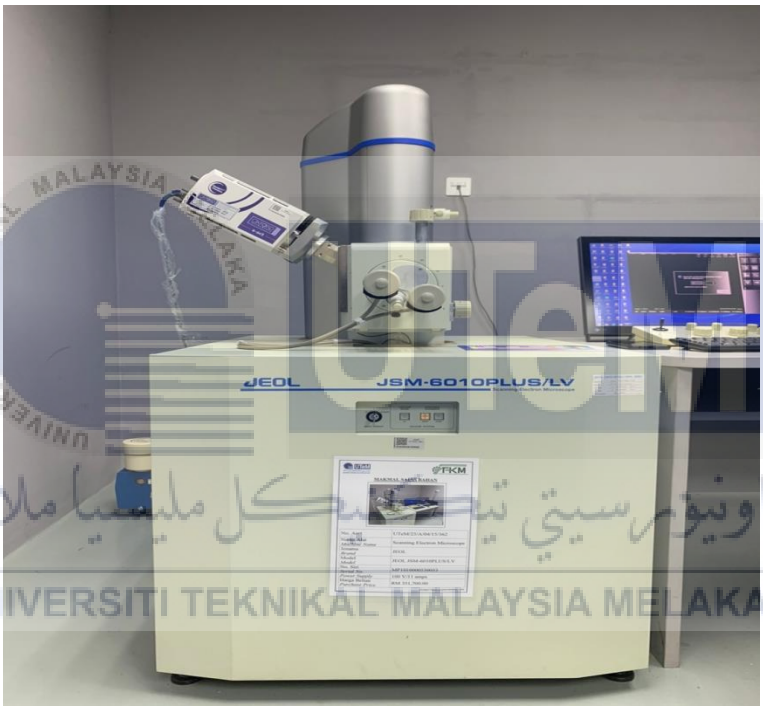

Figure 3.36: SEM Machine located at Fakutli Teknologi Kejuruteraan Mekanikal dan Pembuatan (FTKMP), UTeM.

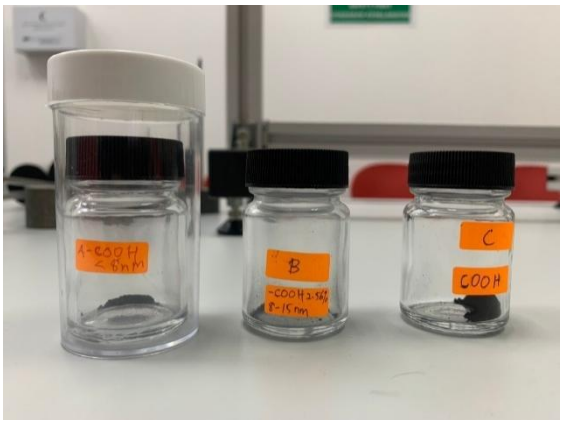

Figure 3.37: Sample delivering for SEM Machine .

3.8 Fourier Transform Infrared Spectroscopy

To determine the chemical bonds of a molecule, Fourier Transform Infrared Spectroscopy (FTIR) generates an infrared absorption spectrum. The spectra offer a sample profile, or a distinct chemical fingerprint, that can be used to examine and screen samples for various components. For the purpose of identifying functional groups and analysing covalent bonding data, FTIR is a potent analytical technique. Figures 3.38 and 3.39 show the sample that was provided for FTIR analysis as well as the FTIR machine that was used for this project.

Figure 3.38: FTIR Machine located at Fakulti Kejuruteraan Pembuatan (FKP), UTeM.

Figure 3.39 Sample delivering for FTIR checking

3.9 Mixing PBS (Phosphate Buffered Saline) With Glucose

To obtain the objective of this project, the PBS solution have to mix with enzyme. Figure 3.40 and Figure 3.41 shows the glucose and its measurement.

Figure 3.40 Glucose

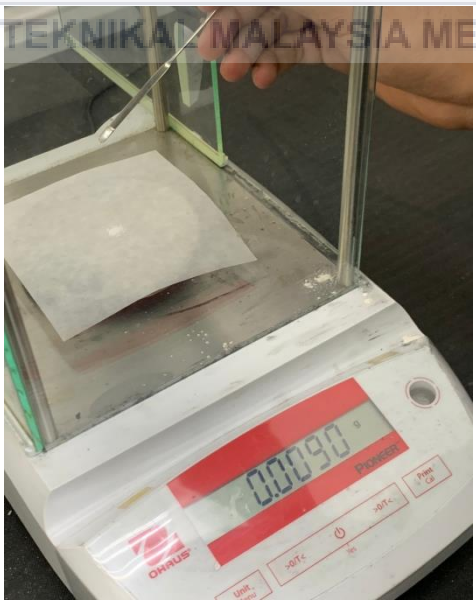

Figure 3.41 Glucose Measurement

CHAPTER 4

RESULTS AND DISCUSSION

4.1 Introduction

This chapter presents the results of Initial Development Of A Nanoelectronic Biosensor For Urea Detection.

4.2Results and Analysis

Figure 4.1 shows the input parameter settings . In cyclic voltammetry input parameters settings , we set for the start potential to -0.5V and the switching potential at 0.5 V . The voltammetric scan rate we put 50 mV/s and 100mV/s . Figure 4.1 and Figure 4.2 shows that we put the Voltammetric scan rate for the input is 50mV/s and 100mV/s .

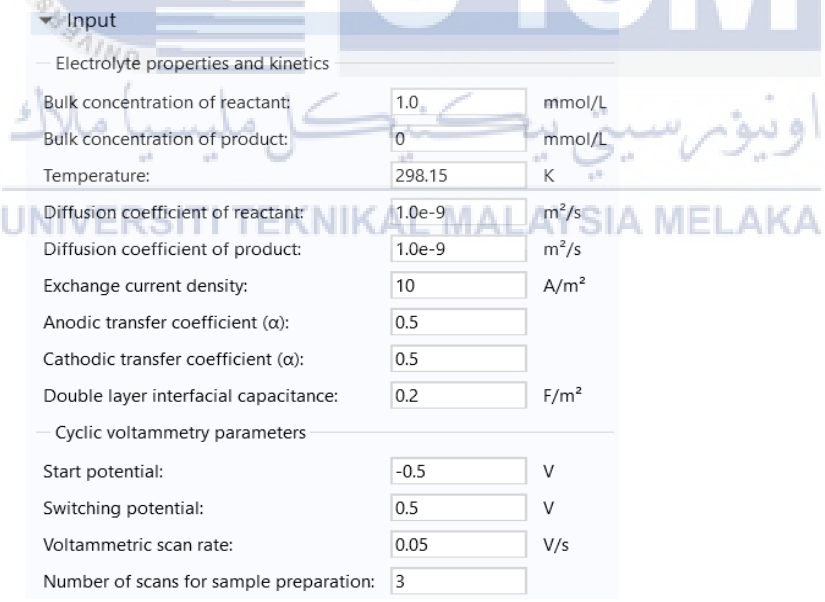

Figure 4.1 Setting parameters input for scan rate 50mV

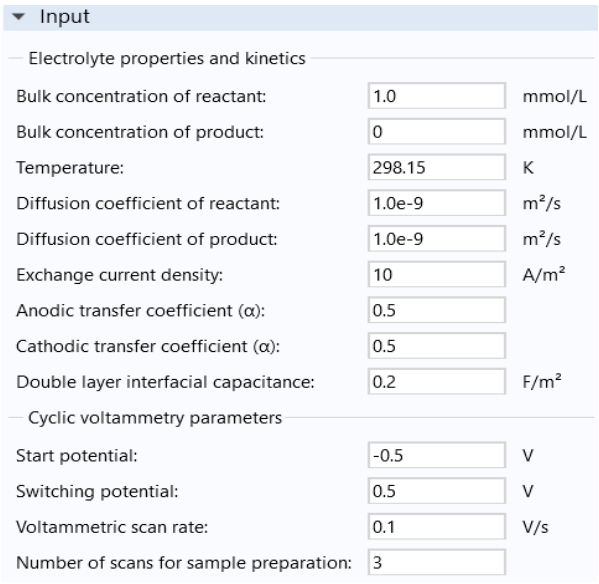

Figure 4.2 Setting parameters input for scan rate 100mV

Figure 4.3 and Figure 4.4 shows the cyclic voltammetry graph and output readings for 50 mV while Figure 4.5 and Figure 4.6 shows the cyclic voltammetry graph and output readings for 100 mV . The graph cyclic voltammetry graph shows the electrical potential (V) versus current density (A/m^2) . From the graph, it shows that the current flows and the electrons move in different movement based on what voltage that enter . From the cyclic voltammetry output reading results , we can see that the current measurement for 100 mV is higher that the output reading results for 50mV. It shows that the higher the scan rate ot the voltammetric , it will fasten the experiment process and make the current output reading higher .

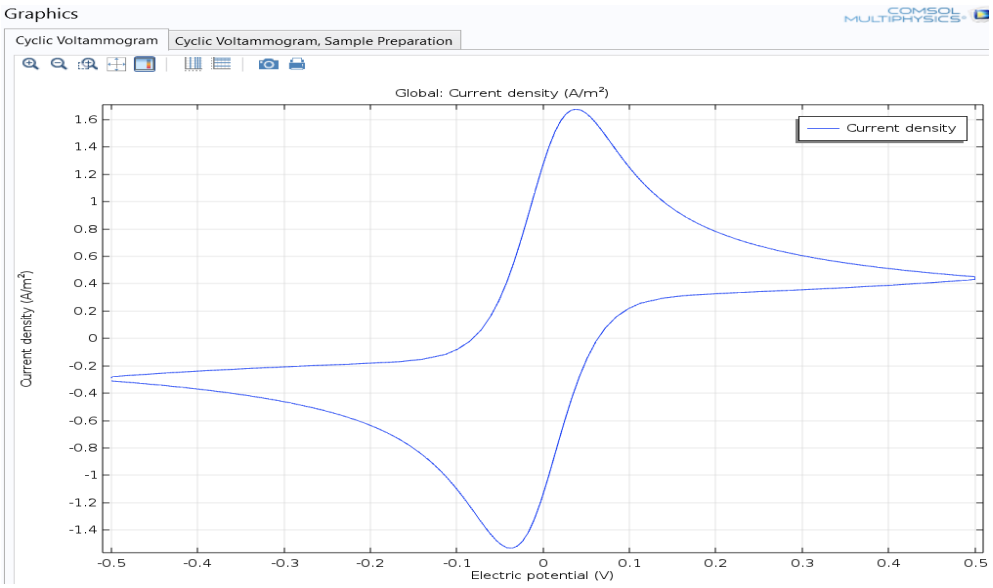

Figure 4.3 Cyclic voltammetry output graph for 50 mV

Results

Peak anodic current:	1.667	A/m²
Electrode potential at peak anodic current:	0.03765	V
Peak cathodic current:	-1.523	A/m²
Electrode potential at peak cathodic current:	-0.03587	V
Potential difference, cathodic vs anodic peak:	0.07352	V

Figure 4.4 Cyclic voltammetry output readings for 50 mV

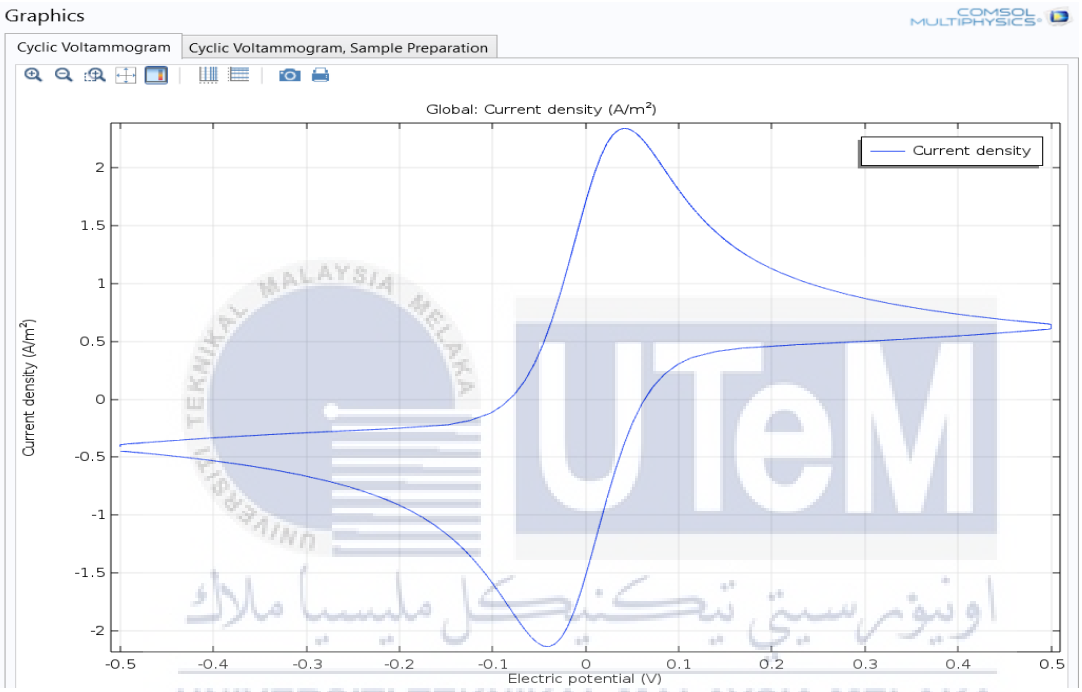

Figure 4.5 Cyclic voltammetry output graph for 100 mV

Results

Peak anodic current:	2.316	A/m²
Electrode potential at peak anodic current:	0.04091	V
Peak cathodic current:	-2.113	A/m²
Electrode potential at peak cathodic current:	-0.03939	V
Potential difference, cathodic vs anodic peak:	0.0803	V

Figure 4.6 Cyclic voltammetry output readings for 100 mV

Figure 4.7 shows the aluminium plate after have been cut . The aluminium plate is cutted by using Bandsaw machine . Figure 4.8 shows the cleaning process of the aluminium plate after have been cutted . It is for cleaning the rusty remains that have on the aluminium.

Figure 4.7 Aluminuim plate after cutted using bandsaw machine

Figure 4.8 Aluminium plate after cleaned

Figure 4.9 , 4.10 and 4.11 shows the finished process after marking and cutting the carbon, stainless steel and copper plate .We marked 1cm in width and 2 cm in length . When done, we cut the metal in size that we marked .

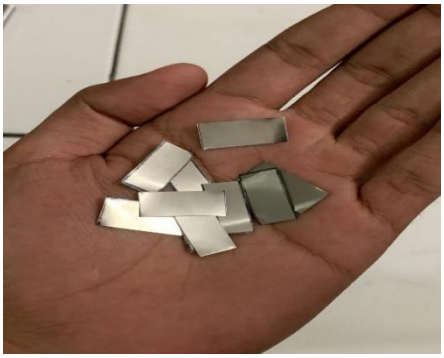

Figure 4.9 Stainless steel after been cut

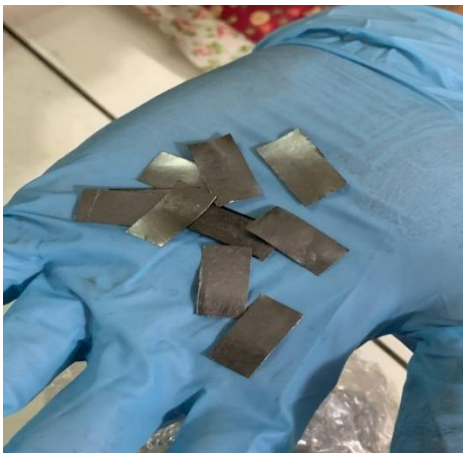

Figure 4.10 Carbon plate after been cut

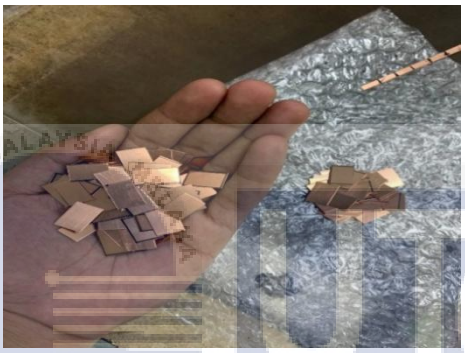

Figure 4.11 Copper plate after been cut

4.3 Electrode Coating Results

4.3.1 Electrode Coating Results On PPy/MWCNT

Each of the electrode is being coated in PPy/MWCNT at 1 minute, 3 minutes and 5 minutes respectively. As shown at the figures below, there are copper, stainless steel, aluminium and carbon that have been coated to PPy/MWCNT solution for 1 minute, 3minutes and 5 minutes. The graph shows the longer the coating process , the thicker the PPY/MWCNT coated on the electrodes .

.

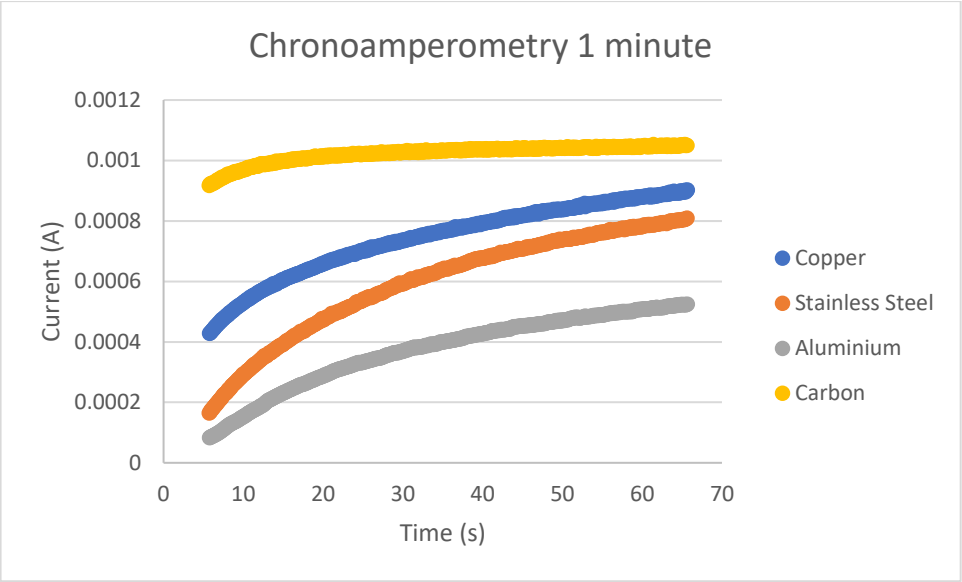

Figure 4.12 Chronoamperomtery on different material at 1 minute

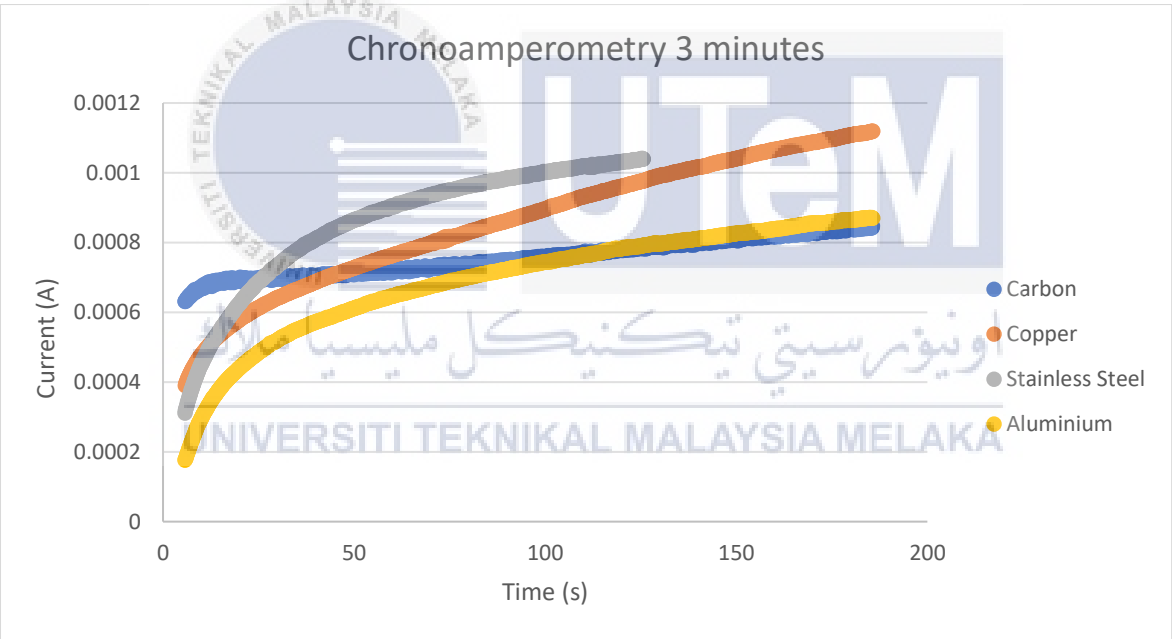

Figure 4.13 Chronoamperomtery on different material at 3 minutes

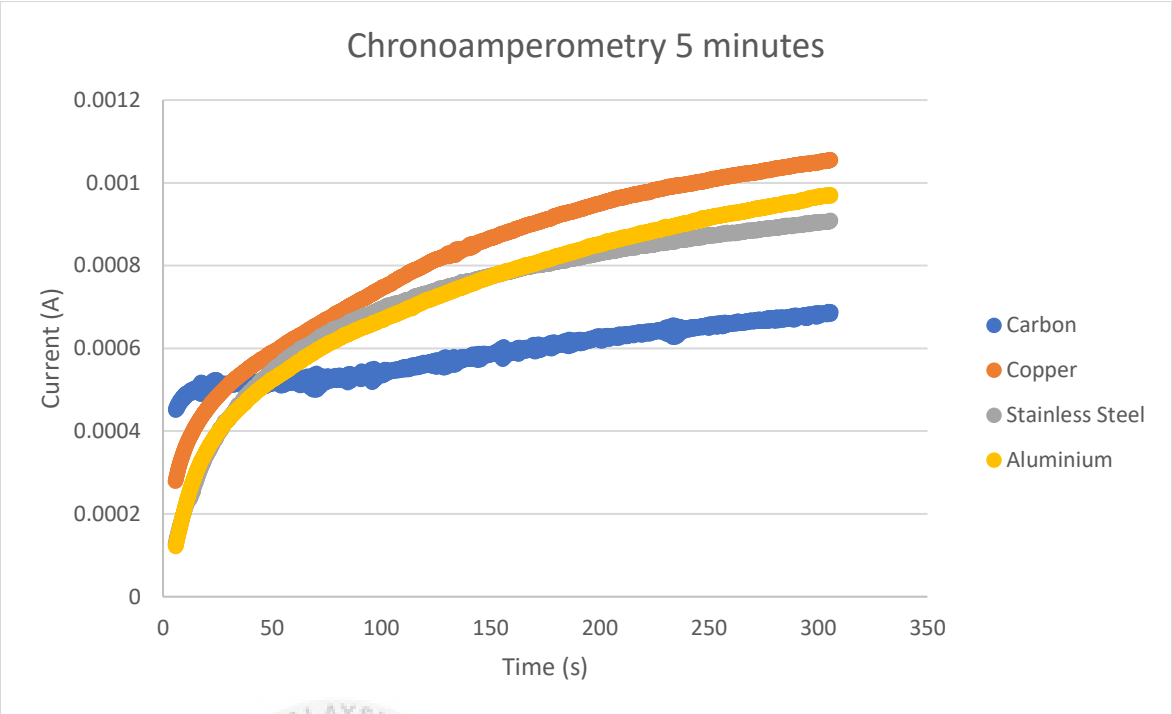

Figure 4.14 Chronoamperomtery on different material at 1 minute

4.3.2 Electrode Coating Results in PBS

Each two of electroode are being use for this process. As shown at the figures below, Figure 4.15 are using two aluminium electrodes for chronoamperometry process. Then, Figure 4.16 are using two stainless steel electrodes for chronoamperometry process. Lastly, Figure 4.17 are using two carbon electrode for chronoamperometry process.

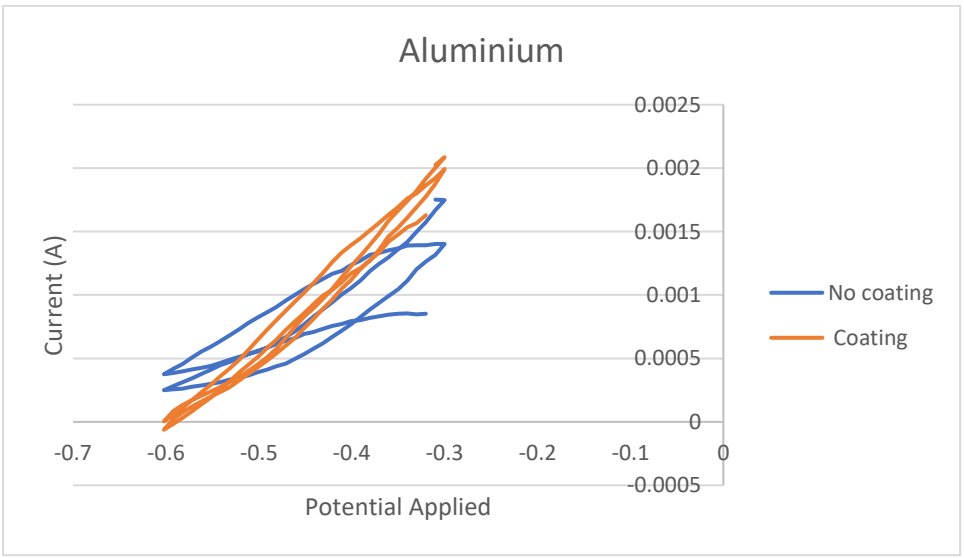

Figure 4.15 Chronoamperomtery on aluminium electrode

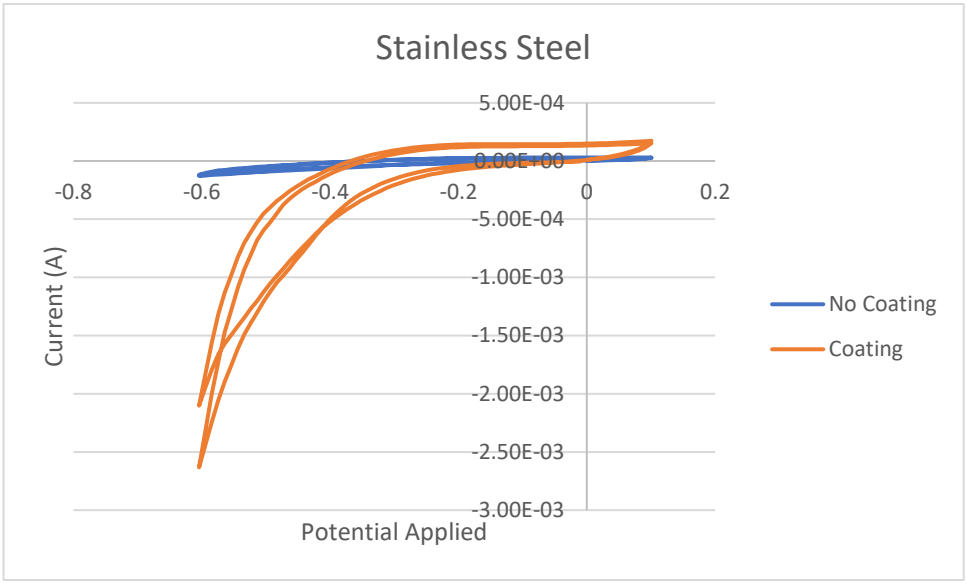

Figure 4.16 Chronoamperomtery on stainless steel electrode

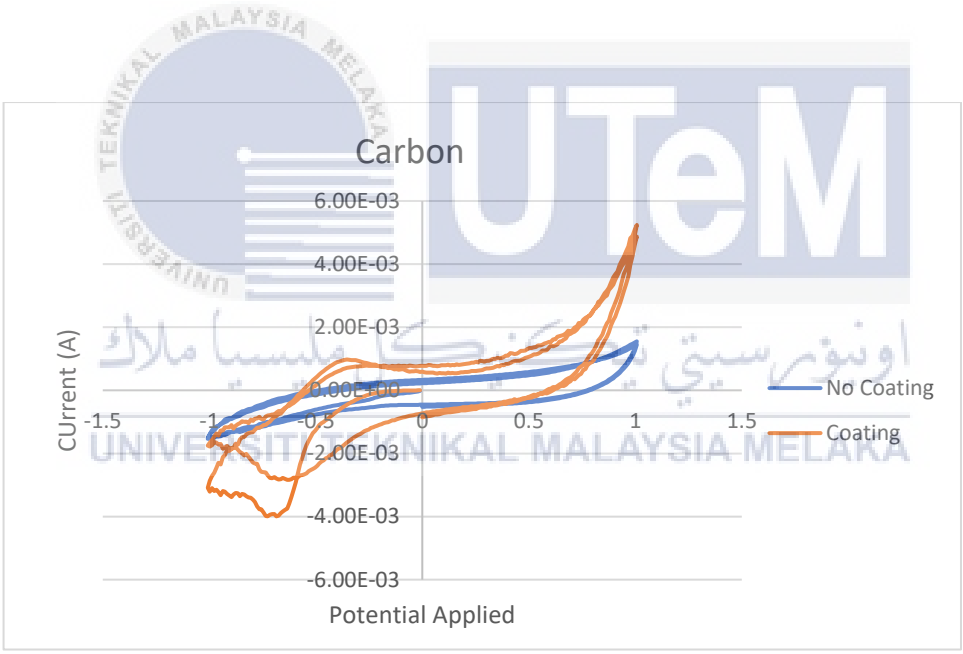

Figure 4.17 Chronoamperomtery on carbon electrode

4.4 Electrode Coating Results On SEM

After coating on PPy/MWCNT, the sample have been sent to SEM at FKM.

4.4.1 Carbon

These are the results after been sent to image checking at SEM. Figure 4.18 shows the SEM image for carbon electrode. Figure 4.19 shows the SEM peak points for carbon electrode. Figure 4.20 shows the SEM properties for carbon electrode.The SEM shows that the oxygen is on the coating that makes the PPY/MWCNT coated on the carbon electrodes.

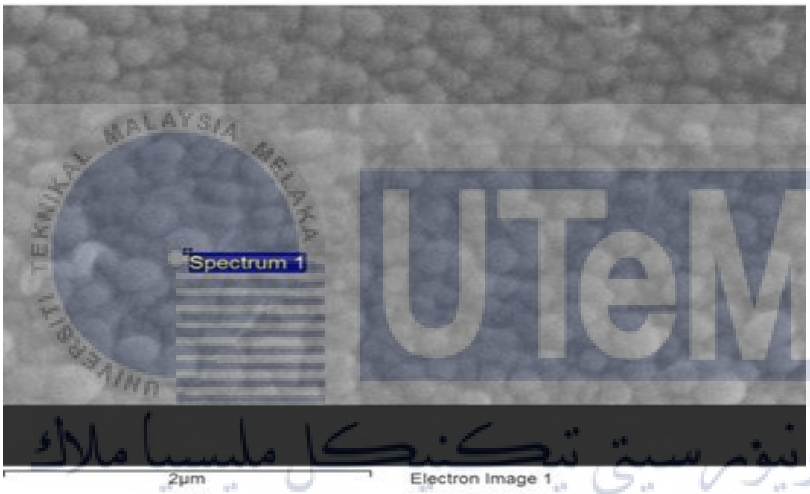

Figure 4.18 SEM image for carbon elecctrode at micrometer

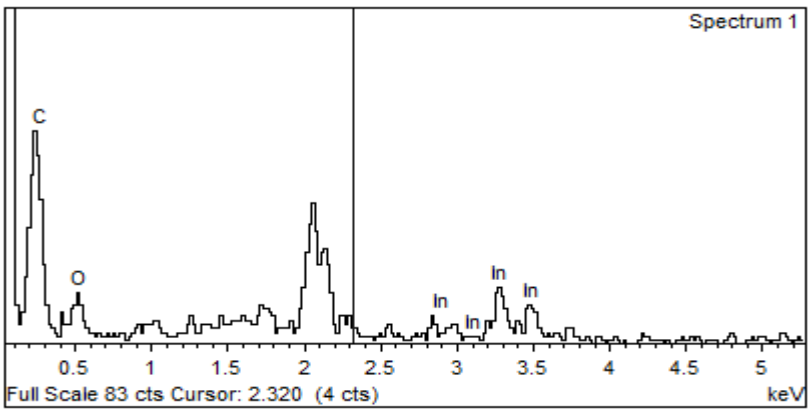

Figure 4.19 SEM peak points for carbon electrode

Spectrum processing :

Peak possibly omitted : 3.000 keV

Processing option : All elements analyzed (Normalised)

Number of iterations = 4

Standard :

C CaCO3 1-Jun-1999 12:00 AM

O SiO2 1-Jun-1999 12:00 AM

Cu Cu 1-Jun-1999 12:00 AM

Element	Weight%	Atomic%
C K	28.99	62.08
O K	7.64	12.28
Cu K	63.37	25.65
Totals	100.00	

Figure 4.20 SEM properties on carbon electrode

4.4.2 Copper

These are the results after been sent to image checking at SEM process. Figure 4.21 shows the SEM image for copper electrode. Figure 4.22 shows the SEM peak points for copper electrode. Figure 4.23 shows the SEM properties for copper electrode. The SEM shows that the oxygen is on the coating that makes the PPY/MWCNT coated on the copper electrodes.

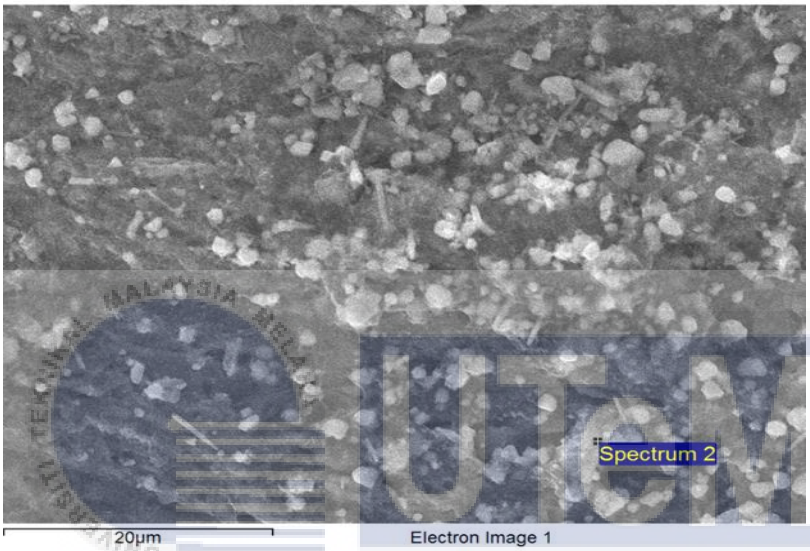

Figure 4.21 SEM image for copper electrode at micrometer

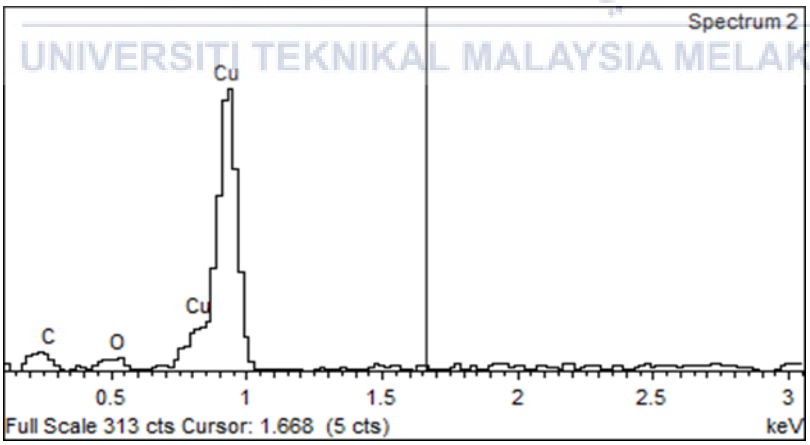

Figure 4.22 SEM peak points for copper electrode

Spectrum processing :

Peak possibly omitted : 3.000 keV

Processing option : All elements analyzed (Normalised)

Number of iterations = 4

Standard :

C CaCO3 1-Jun-1999 12:00 AM

O SiO2 1-Jun-1999 12:00 AM

Cu Cu 1-Jun-1999 12:00 AM

Element	Weight%	Atomic%
C K	28.99	62.08
O K	7.64	12.28
Cu K	63.37	25.65
Totals	100.00	

Figure 4.23 SEM properties on copper electrode

4.4.2 Aluminium

These are the results after been sent to image checking at SEM. Figure 4.24 shows the SEM image for aluminium electrode. Figure 4.25 shows the SEM peak points for aluminum electrode. Figure 4.26 shows the SEM properties for aluminum electrode. The SEM shows that the oxygen is on the coating that makes the PPY/MWCNT coated on the copper electrodes.

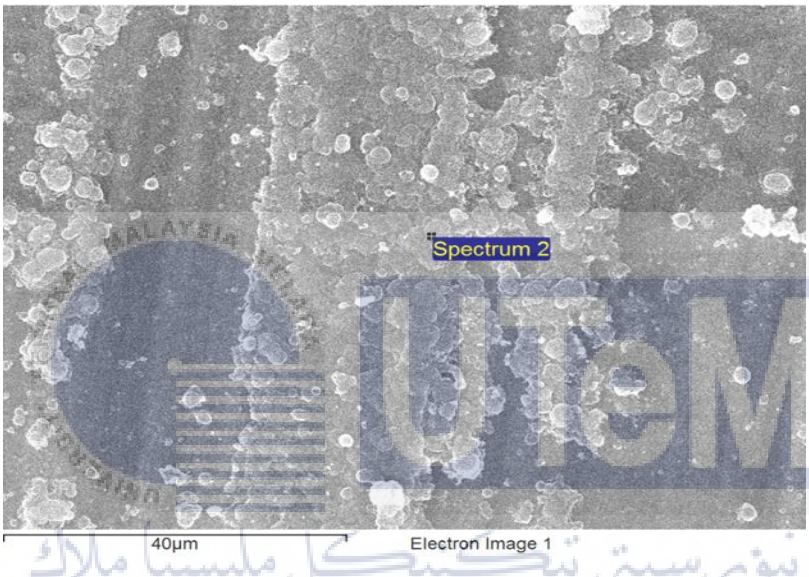

Figure 4.24 SEM image for aluminium electrode at micrometer

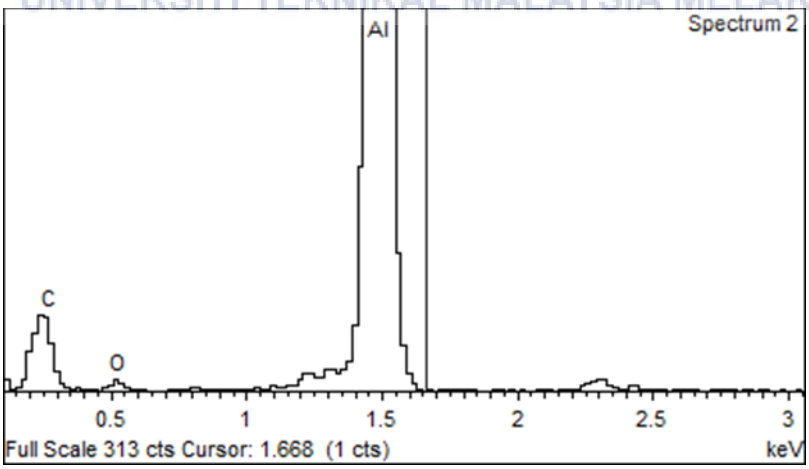

Figure 4.25 SEM peak points for aluminium electrode

Spectrum processing :

No peaks omitted

Processing option : All elements analyzed (Normalised)

Number of iterations = 6

Standard :

C CaCO3 1-Jun-1999 12:00 AM

O SiO2 1-Jun-1999 12:00 AM

Al Al2O3 1-Jun-1999 12:00 AM

Element	Weight%	Atomic%
C K	56.54	72.66
O K	6.30	6.08
Al K	37.16	21.26
Totals	100.00	

Figure 4.26 SEM properties on aluminium electrode

4.5 Electrodes Coating Results on XRD

4.5.1 Stainless Steel + PPy/MWCNT (5 minutes)

These are the results after sending for analyzing and measuring the structure of material at XRD process. Figure 4.27 shows the XRD peak points on stainless steel electrode. After that, Figure 4.28 shows the XRD properties on stainless steel electrode.The results shows changes which is the peak increases and the FWHM become straighter .

Graphics

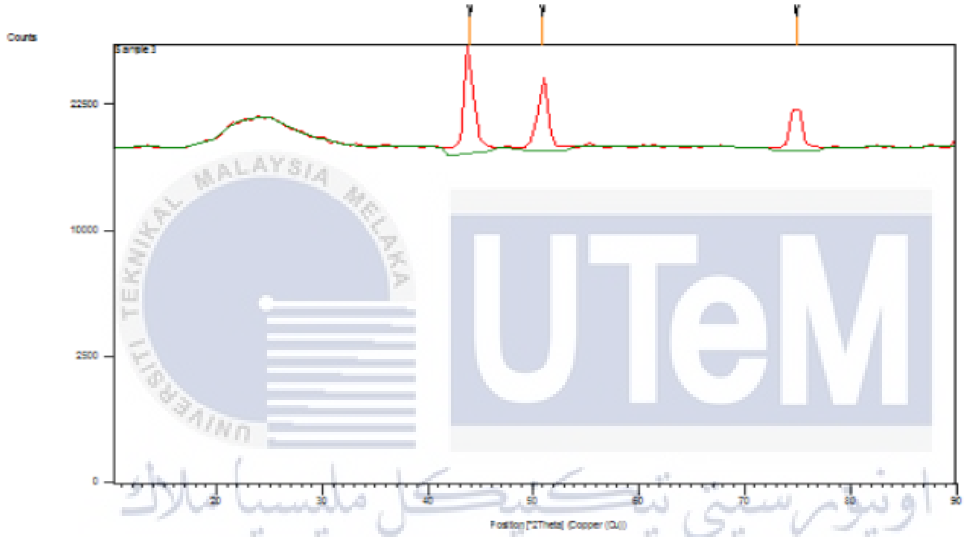

Figure 4.27 XRD peak points on stainless steel electrode

Peak List

Pos.[°2Th.]	Height[cts]	FWHM[°2Th.]	d-spacing[Å]	Rel.Int.[%]
Date: 9/1/2023 Time: 10:36:53 AM		File: Sample 3		
43.8871	12944.50	1.8243	2.06302	100.00
50.9448	8367.19	1.8243	1.79256	64.64
74.9313	5000.19	2.2248	1.26634	38.63

Figure 4.28 XRD properties on stainless steel electrode

4.5.2 Carbon + PPy/MWCNT (5 minutes)

These are the results after sending for analyzing and measuring the structure of material at XRD process. Figure 4.29 shows the XRD peak points on carbon electrode. After that, Figure 4.30 shows the XRD properties on carbon electrode.The peak list shows that carbon peak increased twice after coating .

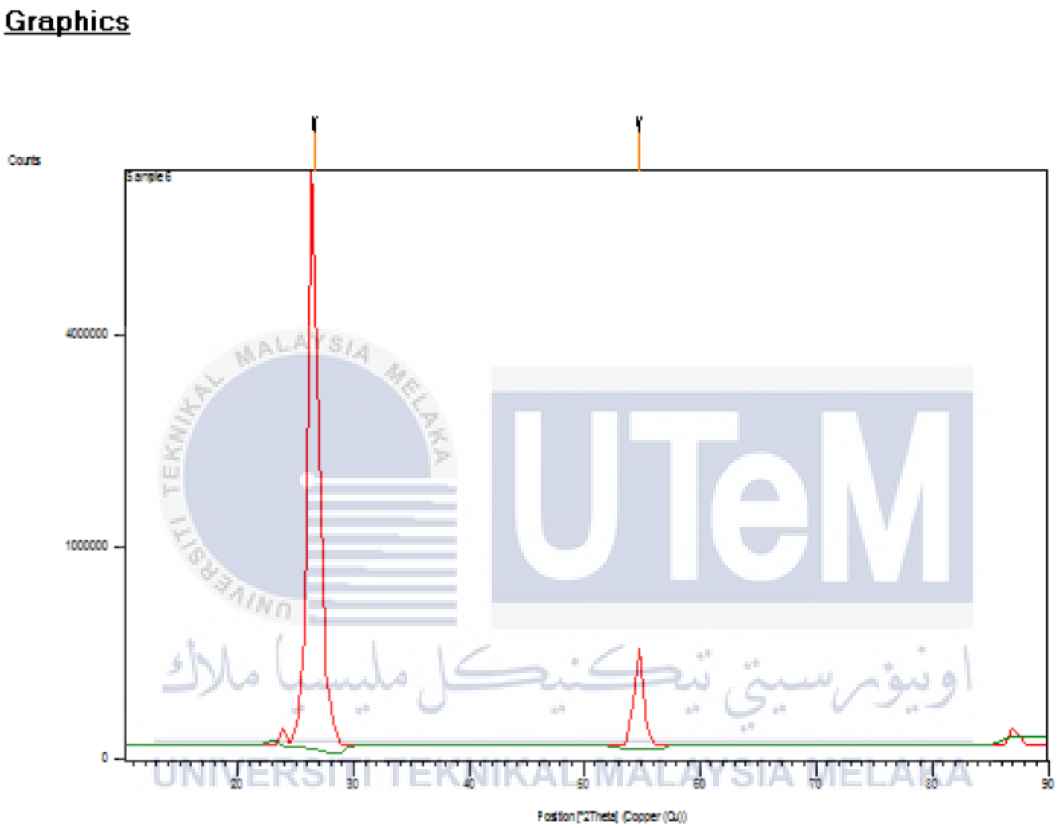

Figure 4.29 XRD peak points on carbon electrode

Peak List

Pos.[°2Th.]	Height[cts]	FWHM[°2Th.]	d-spacing[Å]	Rel.Int.[%]
Date: 9/1/2023 Time: 10:40:16 AM		File: Sample 6		
26.5666	7649359.00	1.8243	3.35531	100.00
54.7250	269714.90	2.2248	1.67595	3.53

Figure 4.30 XRD properties on carbon electrode

4.5.3 Aluminum + PPy/MWCNT (5 minutes)

These are the results after sending for analyzing and measuring the structure of material at XRD process. Figure 4.31 shows the XRD peak points on aluminium electrode. After that, Figure 4.32 shows the XRD properties on aluminium electrode.The graph shows the intensity peak decreases at angle 44 and shows a little peak shows the coating from angle 0 until 30.

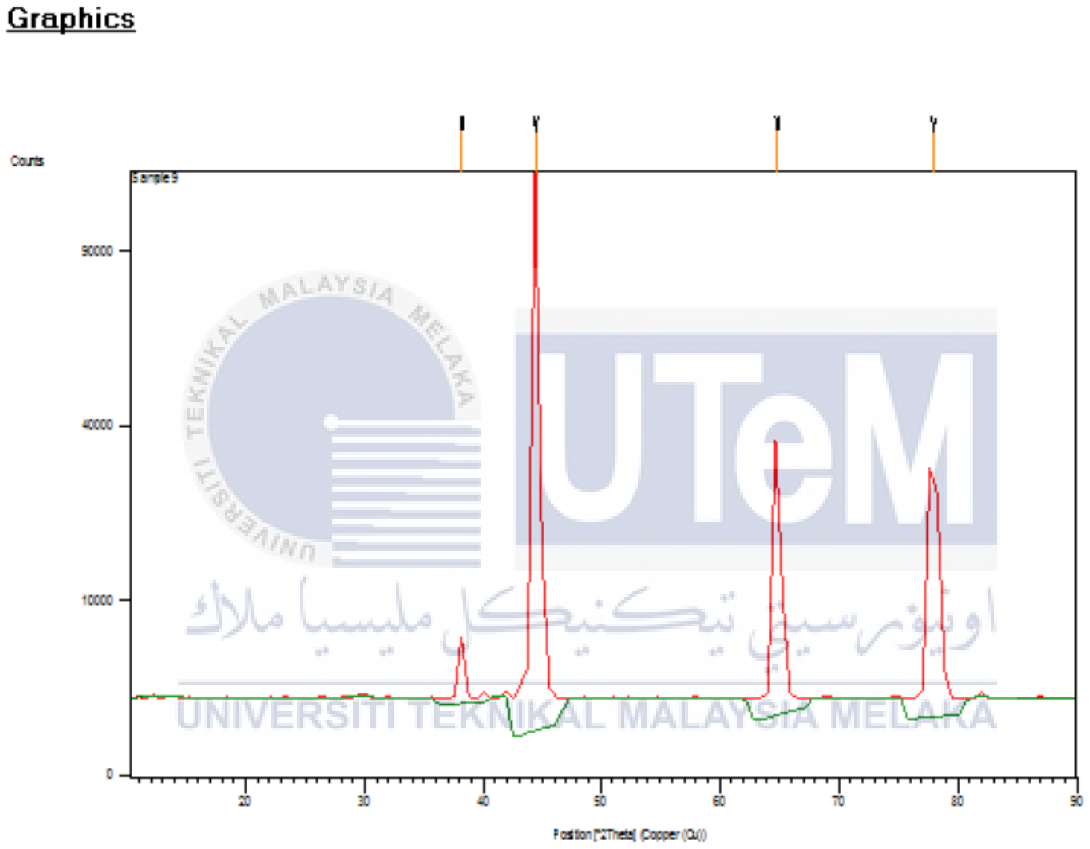

Figure 4.31 XRD peak points on aluminium electrode

Peak List

Pos.[°2Th.]	Height[cts]	FWHM[°2Th.]	d-spacing[Å]	Rel.Int.[%]
Date: 9/1/2023 Time: 10:42:26 AM		File: Sample 9		
38.1693	4644.47	2.4324	2.35786	3.90
44.3946	118998.60	1.8243	2.04061	100.00
64.8637	35067.06	1.8243	1.43752	29.47
78.0002	30970.39	2.2248	1.22401	26.03

Figure 4.32 XRD properties on aluminium electrode

4.6 Electrodes Coating Results on FTIR

These are the results for the sample that have been sent to obtain infrared spectrum at FTIR process. Figure 4.33 shows the data on copper electrode. Figure 4.34 shows the data on carbon electrode. Figure 4.35 shows the data on stainless steel electrode. Figure 4.36 shows the data on aluminium electrode.

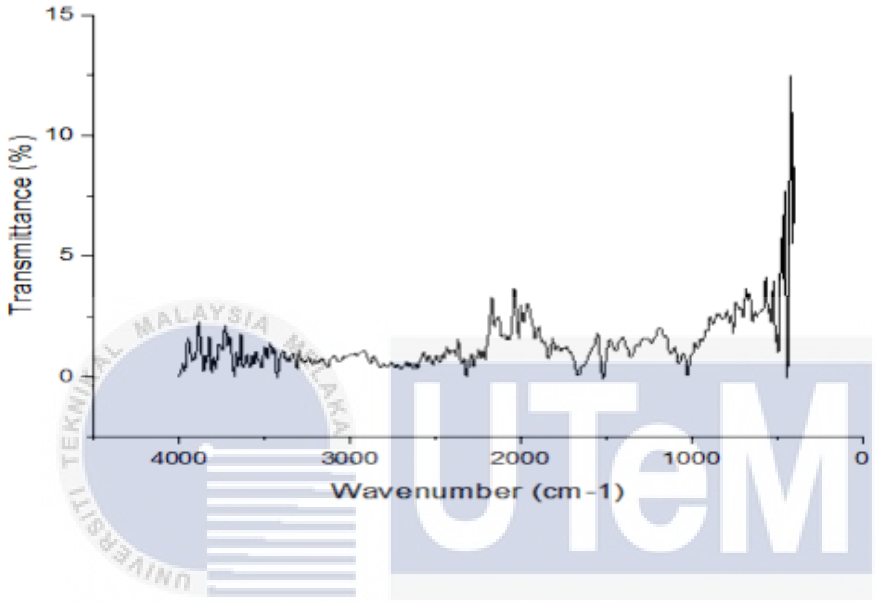

Figure 4.33 FTIR data on copper electrode

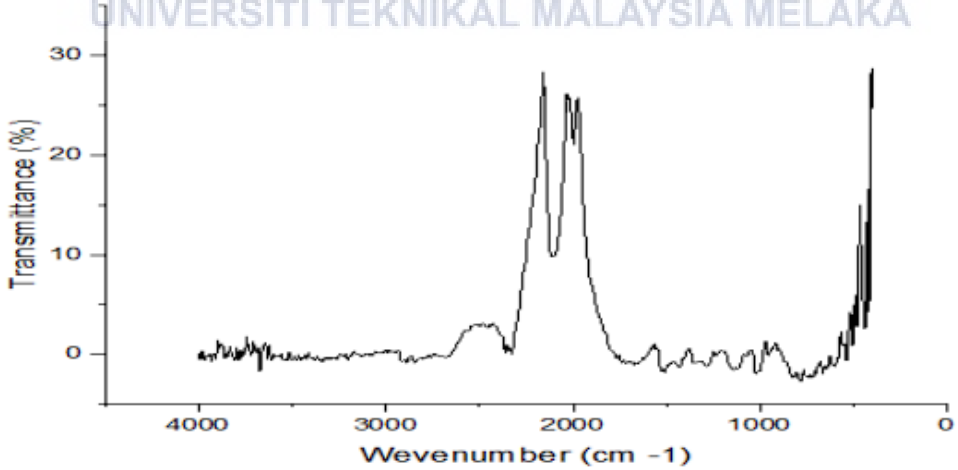

Figure 4.34 FTIR data on carbon electrode

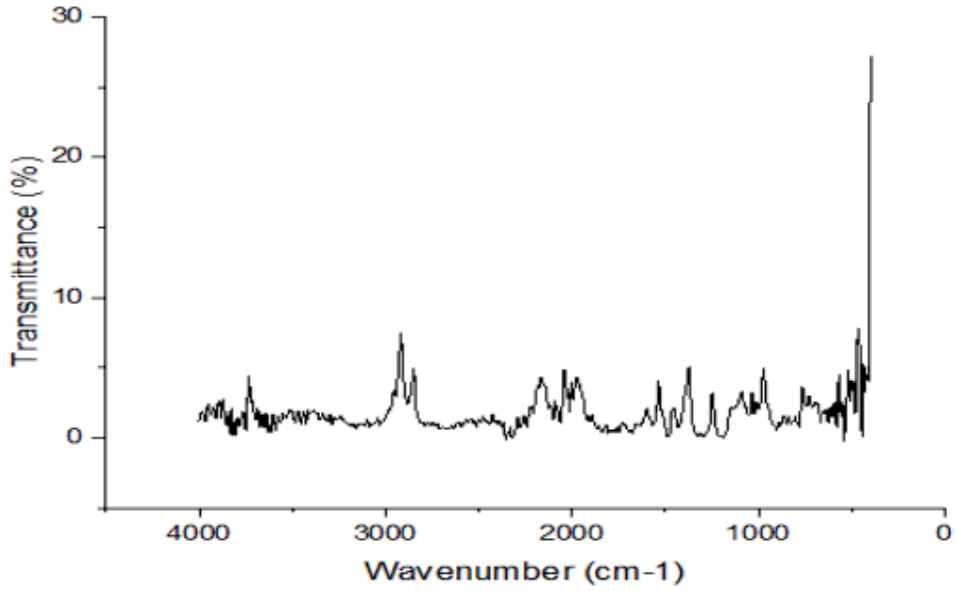

Figure 4.35 FTIR data on stainless steel electrode

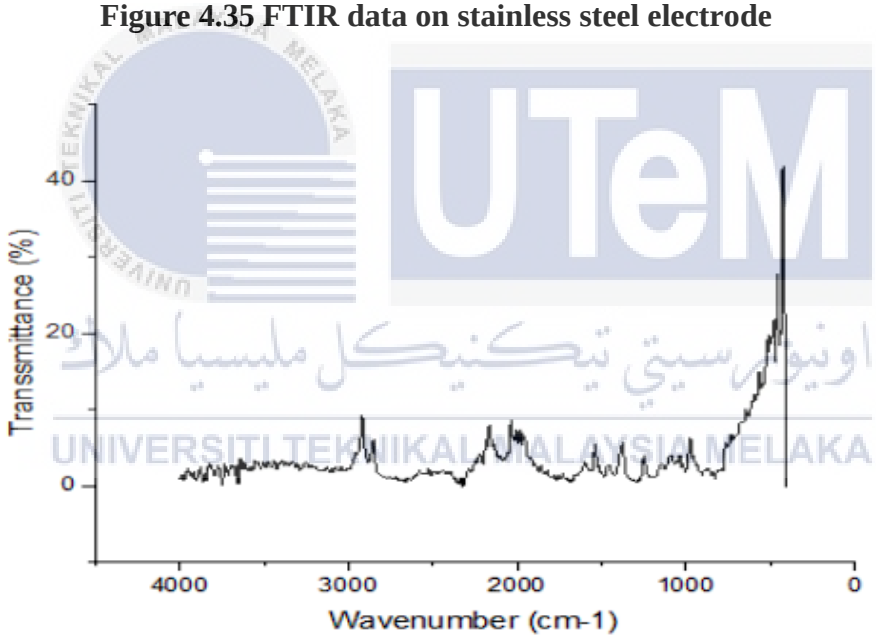

Figure 4.36 FTIR data on aluminum electrode

4.7 Electrodes Coating Results In PBS and Glucose Solution

These are the results for the elctrodes coating in only PBS solution and mix with urea solution. Figure 4.37 shows the result of cyclic voltammetry graph of carbon. Figure 4.38 shows the result of cyclic voltammetry of stainless steel . The cyclic voltammetry shows the reduction and the oxidation process happen on the carbon and the stainless steel when adding urea to the PBS solution . The Cyclic Voltammetry process were able to detect the urea .

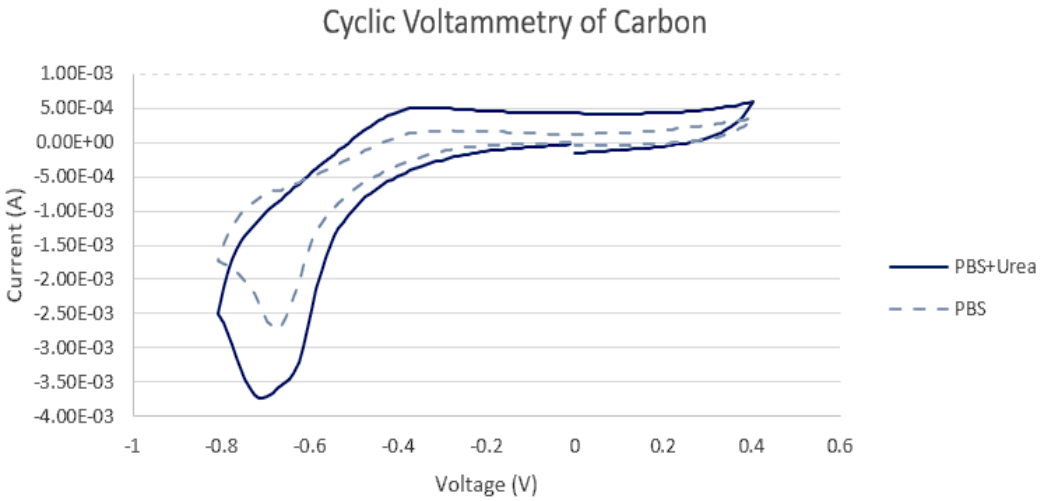

Figure 4.37 Cyclic Voltammetry graph of Carbon

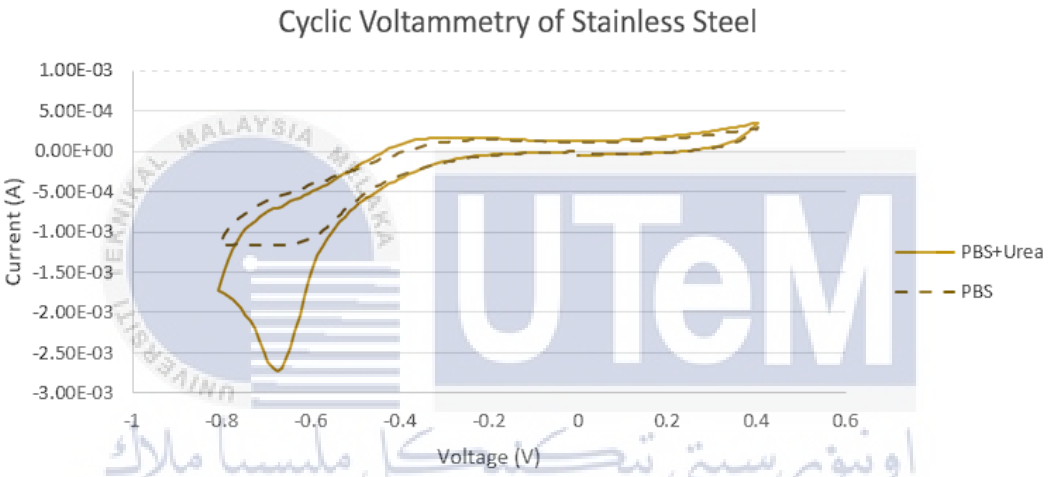

Figure 4.38 Cyclic Voltammetry graph of Stainless Steel

CHAPTER 5

RESULTS AND RECOMMENDATIONS

5.1 Conclusion

Effective urea biosensors can benefit the community and serve as a precautionary measure for victims , preventing death and disease The nanoeletronic urea biosensors is an excellent complement to the early detection the harmful chemical or bilogical agents inside the human body . The devices are made of nanoelectronic materials and can be used to analyze the biological signal in real time. They can also convert the signal into electronic or electrical signals, which can be amplified or quantified. The ability to predict the future use of urea biosensors is a major advance in the field of biosensors. Compared to other technologies, their cost is relatively low and their specificity is high. This findings enable project's objective to be met , and the simulation was completely functional . Finally , the data was able to be nalyzed whic is the redox and the reduction based on the simulations and able to complete the target based on the bachelor degree project objectives . The major findings and insights gathered from the experiments and data analysis would be described at the end of the research report on cyclic voltammetry . This might contain information such as carbon ,aluminium , copper and stainless steel electrode . Futhermore , the conclusion may explain the researchers larger implication as well as potential suggestion for further investigation.

5.2 Future Works

There are several ongoing research efforts in the development of nanoelectronic biosensors for urea detection. One approach is to use nanoparticles, such as gold or silicon, as the sensing element in the biosensor. These nanoparticles can be functionalized with urea-specific enzymes or antibodies, which will bind to urea molecules and generate a measurable electrical signal. Another approach is to use carbon nanotubes or graphene as the sensing element, which can also be functionalized with urea-specific enzymes or antibodies. These nanoelectronic biosensors are expected to have high sensitivity, specificity, and stability, making them useful for continuous urea monitoring in patients with Chronic Kidney Disease

(CKD) . However, these biosensors are still in the research and development stage and more work is needed before they can be widely used in clinical applications.

5.3 Project Potential

Commercialization of nanoelectronic biosensors entails developing, manufacturing, and selling these sensors for a variety of applications such as medical diagnostics, environmental monitoring, and food safety. Typically, the process includes research and development to increase the performance and reliability of the sensors while also lowering their cost and size. Once designed and tested, a biosensors may be mass-produced and offered to a variety of sectors and end-users. A nanoelectronic biosensor's commercial success will be determined by parameters such as its accuracy, sensitivity, and costs, as well as the size of the target market and the amount of competition.

REFERENCES

[1] Fapyane, D., Berillo, D., Marty, J. L., & Revsbech, N. P. (2020). Urea biosensor based on a CO2 microsensor. *ACS Omega*, *5*(42), 27582–27590. https://doi.org/10.1021/acsomega.0c04146

[2]Sin, M. L., Mach, K. E., Wong, P. K., & Liao, J. C. (2014). Advances and challenges in biosensor-based diagnosis of infectious diseases. In *Expert Review of Molecular Diagnostics* (Vol. 14, Issue 2, pp. 225–244). https://doi.org/10.1586/14737159.2014.888313

[30]Zucolotto, V. (2020). Specialty Grand Challenges in Biosensors. *Frontiers in Sensors, 1*. https://doi.org/10.3389/fsens.2020.00003

[4]Bhalla, N., Jolly, P., Formisano, N., & Estrela, P. (2016). Introduction to biosensors. *Essays in Biochemistry*, *60*(1), 1–8. https://doi.org/10.1042/EBC20150001

[5]Tetyana, P., Morgan Shumbula, P., & Njengele-Tetyana, Z. (2021). Biosensors: Design, Development and Applications. In *Nanopores*. IntechOpen. https://doi.org/10.5772/intechopen.97576

[6]Akmar Jamil, N., Bariyah Khairulazdan, N., Susthitha Menon, P., Rifqi Md Zain, A., Azlan Hamzah, A., & Yeop Majlis, B. (n.d.). *Graphene-MoS_2 SPR-based biosensor for urea detection*.

[7] Institute of Electrical and Electronics Engineers, & Institute of Electrical and Electronics Engineers. Turkey Section. (n.d.). *TIPTEKNO'21 : Tıp Teknolojileri Kongresi : 4-6 Kasım, 2021, IC Green Palace Hotel Antalya.*

[8] Chou, J. C., Wu, C. Y., Kuo, P. Y., Lai, C. H., Nien, Y. H., Wu, Y. X., Lin, S. H., & Liao, Y. H. (2019). The Flexible Urea Biosensor Using Magnetic Nanoparticles. *IEEE Transactions on Nanotechnology*, *18*, 484–490. https://doi.org/10.1109/TNANO.2019.2895137

[9] Vaghela, C., Kulkarni, M., Aiyer, R., & Karve, M. (2018). LED-Based Portable Optical Biosensor for Measurement of Serum Urea Levels Using Urease Immobilized Agarose-Guar Gum Composite Film. *IEEE Sensors Journal*, *18*(17), 7273–7280. https://doi.org/10.1109/JSEN.2018.2850909.

[10] Nien, Y. H., Su, T. Y., Ho, C. S., Chou, J. C., Lai, C. H., Kuo, P. Y., Kang, Z. X., Dong, Z. X., Lai, T. Y., & Wang, C. H. (2020). The Analysis of Potentiometric Flexible Arrayed Urea Biosensor Modified by Graphene Oxide and γ-Fe2O3Nanoparticles. *IEEE*

Transactions on Electron Devices, *67*(11), 5104–5110. https://doi.org/10.1109/TED.2020.3023067

[11]Kuo, P. Y., Dong, Z. X., & Chen, Y. Y. (2021). The Hysteresis Reduction Approach for Urea Biosensor Modified by Silver Nanoparticles. *IEEE Transactions on Nanotechnology*, *20*, 311–320. https://doi.org/10.1109/TNANO.2021.3070443

[12] Cheng, L., Zheng, W., Li, L., & Zhang, Y. N. (2021). Highly-Sensitive SPR Urea Biosensor Based on Urease Immobilized in Metal-Organic Zeolite Framework. *2021 19th International Conference on Optical Communications and Networks, ICOCN 2021*. https://doi.org/10.1109/ICOCN53177.2021.9563719

[13] Kuo, P. Y., Dong, Z. X., & Chen, Y. Y. (2021). The Stability Analysis of Potentiometric Urea Biosensor under Microfluidic System and Remote Measurement. *IEEE Transactions on Instrumentation and Measurement*, *70*. https://doi.org/10.1109/TIM.2021.3075036

[14] Nien, Y. H., Su, T. Y., Chou, J. C., Lai, C. H., Kuo, P. Y., Lin, S. H., Lai, T. Y., & Rangasamy, M. (2021). Investigation of Flexible Arrayed Urea Biosensor Based on Graphene Oxide/Nickel Oxide Films Modified by Au Nanoparticles. *IEEE Transactions on Instrumentation and Measurement*, *70*. https://doi.org/10.1109/TIM.2020.3017941

[15] IEEE Malaysia Section. Electron Devices Chapter, Universiti Kebangsaan Malaysia. Institute of Microengineering and Nanoelectronics, & Institute of Electrical and Electronics Engineers. (n.d.). *2018 IEEE International Conference on Semiconductor Electronics (ICSE2018) : proceedings : 15-17 August 2018, Pullman Kuala Lumpur City Centre Hotel & Residence, Kuala Lumpur, Malaysia*.

[16] Hung, L. C., Lin, Z. Y., & Chou, Y. N. (2021). Glass-based fluorescent immunobiosensor used for urea albumin fast detection. *2021 IEEE International Conference on Consumer Electronics-Taiwan, ICCE-TW 2021*. https://doi.org/10.1109/ICCE-TW52618.2021.9603243

[17] Fapyane, D., Berillo, D., Marty, J. L., & Revsbech, N. P. (2020). Urea biosensor based on a CO2 microsensor. *ACS Omega*, *5*(42), 27582–27590. https://doi.org/10.1021/acsomega.0c04146

[18] Hussain, S., & Park, S. Y. (2020). Sweat-Based Noninvasive Skin-Patchable Urea Biosensors with Photonic Interpenetrating Polymer Network Films Integrated into PDMS Chips. *ACS Sensors*, *5*(12), 3988–3998. https://doi.org/10.1021/acssensors.0c01757

[19] Li, J., Wan, J., Han, M., & Zhang, H. (2021). Design and fabrication of a multimode optical fiber surface plasmon resonance urea biosensor††This work was supported by the

National Natural Science Foundation of China (Grant No. 61674004). *Proceedings of the 16th Annual IEEE International Conference on Nano/Micro Engineered and Molecular Systems, NEMS 2021*, 1686–1690. https://doi.org/10.1109/NEMS51815.2021.9451341
[20]Singh, S., Sharma, M., & Singh, G. (2021). Recent advancementsin urea biosensors for biomedical applications. In *IET Nanobiotechnology* (Vol. 15, Issue 4, pp. 358–379). John Wiley and Sons Inc. https://doi.org/10.1049/nbt2.12050
[21] Encyclopedia of Tribology. (2013). In *Encyclopedia of Tribology*. Springer US. https://doi.org/10.1007/978-0-387-92897-5
[22] Han, Y., Chen, P., Xia, Y., Huang, S., Chen, W., & Lu, W. (2019). Electrodeposition of polypyrrole on He plasma etched carbon nanotube films for electrodes of flexible all-solid-state supercapacitor. *Journal of Solid State Electrochemistry*. https://doi.org/10.1007/s10008-019-04242-4
[23] Abyzov, A. M., Kidalov, S. v., & Shakhov, F. M. (2012). High thermal conductivity composite of diamond particles with tungsten coating in a copper matrix for heat sink application. *Applied Thermal Engineering*, *48*, 72–80. https://doi.org/10.1016/j.applthermaleng.2012.04.063.
[24] Cialone, M., Fernandez-Barcia, M., Celegato, F., Coisson, M., Barrera, G., Uhlemann, M., Gebert, A., Sort, J., Pellicer, E., Rizzi, P., & Tiberto, P. (2020). A comparative study of the influence of the deposition technique (electrodeposition versus sputtering) on the properties of nanostructured Fe70Pd30 films. *Science and Technology of Advanced Materials*, *21*(1), 424–434. https://doi.org/10.1080/14686996.2020.1780097
[25] Saeedfar, K., Heng, L. Y., Ling, T. L., & Rezayi, M. (2013). Potentiometric urea biosensor based on an immobilised fullerene-urease bio-conjugate. *Sensors (Switzerland)*, *13*(12), 16851–16866. https://doi.org/10.3390/s131216851
[26] Jakhar, S., & Pundir, C. S. (2018). Preparation, characterization and application of urease nanoparticles for construction of an improved potentiometric urea biosensor. *Biosensors and Bioelectronics*, *100*, 242–250. https://doi.org/10.1016/j.bios.2017.09.005
[27] Fenoy, G. E., Marmisollé, W. A., Azzaroni, O., & Knoll, W. (2020). Acetylcholine biosensor based on the electrochemical functionalization of graphene field-effect transistors. *Biosensors and Bioelectronics*, *148*. https://doi.org/10.1016/j.bios.2019.111796
[28] Yang, Z., Qin, T., Niu, Y., Zhang, Y., Zhang, C., Li, P., Zhu, M., Jia, Y., & Li, Q. (2020). Flexible visible-light-driven photoelectrochemical biosensor based on molecularly imprinted nanoparticle intercalation-modulated graphene fiber for ultrasensitive urea detection. *Carbon*, *157*, 457–465. https://doi.org/10.1016/j.carbon.2019.10.061

[29] Dervisevic, M., Dervisevic, E., Senel, M., Cevik, E., Yildiz, H. B., & Camurlu, P. (2017). Construction of ferrocene modified conducting polymer based amperometric urea biosensor. *Enzyme and Microbial Technology*, *102*, 53–59. https://doi.org/10.1016/j.enzmictec.2017.04.002

[30] "Scanning Electron Microscope - Radiological and Environmental Management - Purdue University," Purdue.edu, 2019.

[31] "Scanning Electron Microscopy," Nanoscience Instruments, Mar. 2022.

[32] "FTIR Analysis | RTI Laboratories," Rtilab.com, 2015.

[33] "FTIR Detectors: Basics," Thermofisher.com, 2015.

[34] "X-ray diffraction (XRD) basics and application," Chemistry LibreTexts, Apr. 14, 2019.

[35] "What is a Potentiostat and how does it work? ", Pine Research Instrumentation , Apr. 07, 2021.

[36] "COMSOL Multiphysics®," COMSOL, 2022.

[37] "M. Brashem, Inc.," Mbrashem, Jan. 19, 2021.

[38] "Aluminium - Element information, properties and uses | Periodic Table," Rsc.org, 2017.

[39] Dielectric Manufacturing, "Copper," Dielectric Manufacturing, Feb. 27, 2019.

[40] "Stainless Steel Characteristics: Grades, Properties & Applications," Eagle Stainless, Jun. 17, 2019

[41] "Sheet Metal Hand Notcher.". Available.

[42] "Shear," Maine. edu, 2022.

[43] Makefromwood.com, Jun. 12, 2020.

APPENDICES

Appendix A : Project Gantt Chart Bachelor Degree Project 1

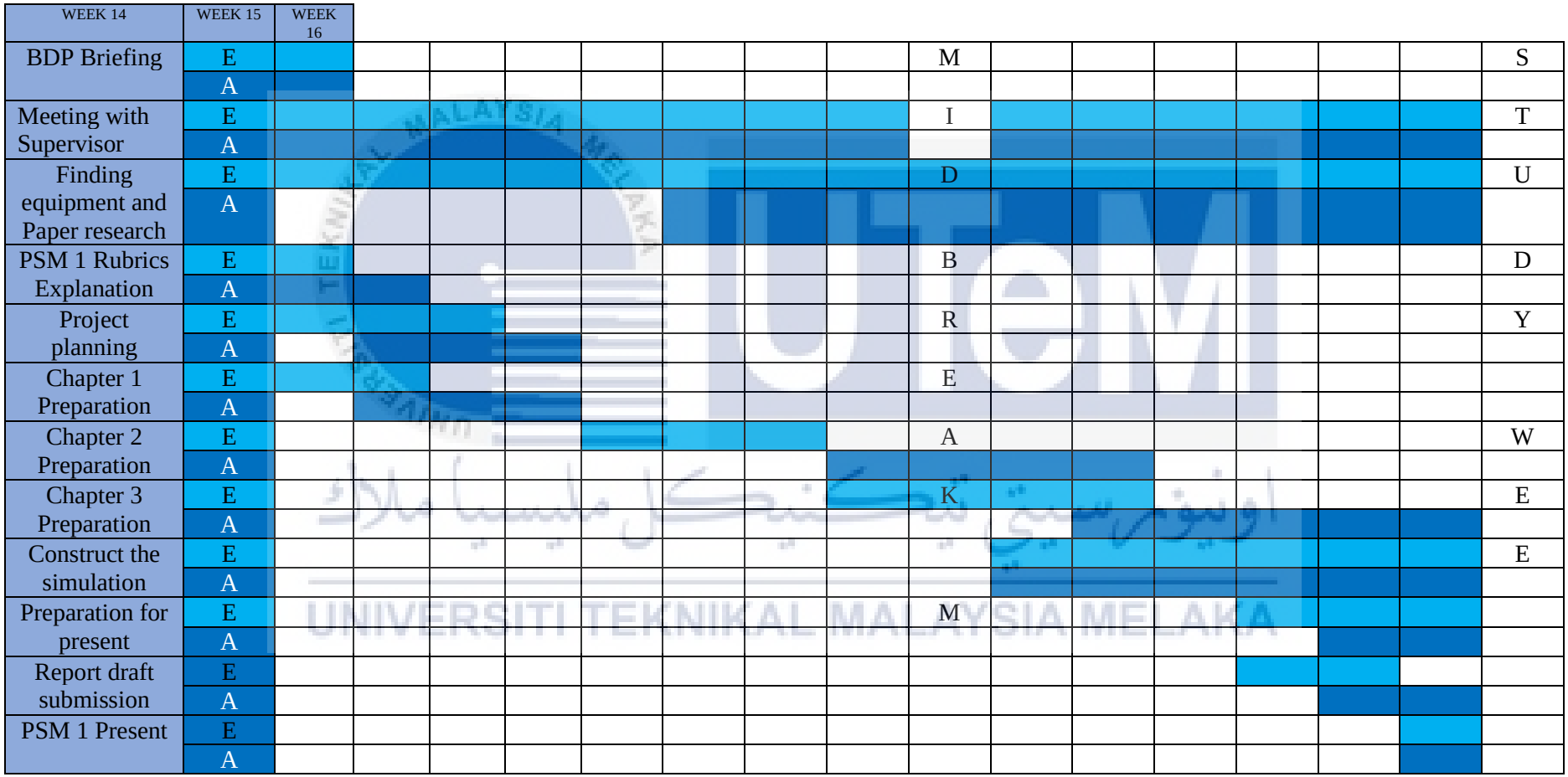

Notes: E- Expected A-Actual

Appendix B : Project Gantt Chart Bachelor Degree Project 2

PROJECT ACTIVITIES	STATUS	WEEK 1	WEEK 2	WEEK 3	WEEK 4	WEEK 5	WEEK 6	WEEK 7	WEEK 8	WEEK 9	WEEK 10	WEEK 11	WEEK 12	WEEK 13	WEEK 14	WEEK 15	WEEK 16
Draft Material List	E									M							S
	A																
Meeting with Supervisor	E									I							T
	A																
Doing lab experiment	E									D							U
	A																
Analyse Result	E									B							D
	A																
Complete Chapter 4 : Result and Discussion	E									R							Y
	A																
Complete Chapter 5:Conclusion	E									E							
	A																
Submit Draft Report	E									A							W
	A																
Prepare Project Poster	E									K							E
	A																
Preparation for presentation	E																E
	A									S							
Presentation	E																K
	A									E							
Submit Final Report	E																
	A									M							

Notes: E- Expected A-Actual